Performance investigation of a novel low-carbon solar-assisted multi-source heat pump heating system demonstrated in a public building in Hull

Yunhai Li [a], Zhaomeng Li [b,d], Zhiying Song [b], Yi Fan [c], Xudong Zhao [a, *, **], Jing Li [a, *, **]

[a] Centre for Sustainable Energy Technologies, University of Hull, Cottingham Road, Hull, HU6 7RX, UK

[b] Department of Thermal Science and Energy Engineering, University of Science and Technology of China, Hefei 230026, China

[c] College of Energy and Mechanical Engineering, Shanghai University of Electric Power, Shanghai 201306, China

[d] Shanghai Micro Electronics Equipment (Group) CO., LTD, Shanghai 201203, China

* Corresponding authors. Tel.: +44-01482466684 (X. Zhao), +44-01482463611 (J. Li).

E-mail addresses: Xudong.Zhao@hull.ac.uk (X. Zhao), Jing.Li@hull.ac.uk (J. Li).

** The two authors have the same contribution to this study.

Abstract: Global climate change has raised great attention from governments and prompted a wave of low-carbon technological innovation. The Hull City Council promised to lead the carbon neutrality, becoming fully carbon neutral by 2030. Following the carbon-neutral strategy, a novel low-carbon solar-assisted multi-source heat pump heating system (LSMHS) is proposed and demonstrated in Hull Central Library by replacing the library's original gas boiler heating system (GBHS). The LSMHS integrates eight novel multi-throughout-flowing solar collector arrays with an innovative two-stage heat recovery heat pump which can automatically switch different operation modes according to weather conditions. The practical operation results revealed that the LSMHS maximized the advantages of each component and achieved a high monthly average system COP_{sys} ranging from 2.12 to 2.68 in the three-month demonstration. Eventually, the LSMHS provided a bill saving of 0.73% with a significant carbon reduction of 63.69% when compared to the GBHS in practice, achieving an equivalent bill saving of £6.7 for every tone of carbon reduction. The remarkable demonstration results showcased the application potential of the novel LSMHS and gave valuable guidance for low-carbon building heating.

Keywords: Practical demonstration; solar-assisted heat pump; eco-economic performance; heating decarbonization.

Nomenclature

Symbols		**Subscripts**	
T	Real-time temperature (ºC)	i	Time step
$\bar{T}$	Average temperature(ºC)	w	Water
R	Real-time solar radiation (W/m^2)	out	Outdoor
$\bar{R}$	Average solar radiation (W/m^2)	in	indoor
Q	Heating capacity (W)	inlet	Water inlet
W	Power consumption (W)	outlet	Water outlet
U	Voltage (V)	sys	System
I	Current (A)	**Abbreviations**	
∂	Thermal efficiency	HP	Heat pump
E	Energy consumption (kWh)	SAHP	Solar-assisted heat pump
c	Special heating capacity of water(kJ/kg/ºC)	THRHP	Two-stage heat recovery heat pump
ρ	Density of water (kg/m^3)	LSMHS	Low-carbon solar-assisted multi-source heat pump heating system
$\dot{v}$	Volume flow rate of water (m^3/h)	MFSC	Multi-throughout-flowing solar collector
θ	Power factor	FC	Fan coil
HG	Heat generation of heat pump (kWh)	SC	Solar collector
HC	Heat collection of solar collectors (kWh)	COP	Coefficient of Performance
HS	Heat supply of fan coils (kWh)		

1. **Introduction**

The world is facing a major challenge of climate change, which is caused by ingrained dependence on fossil fuels and increasing levels of carbon emissions. One of the largest contributors to these emissions is the heating of buildings, accounting for 48% of global energy consumption, and leading to 40% of global carbon emissions [1]. To effectively address climate issues, countries around the world are placing increasing importance on innovative low-carbon energy-efficient heating technologies, seeking new game-changing, scalable, and commercially viable technologies to accomplish the national carbon-neutral goals. In line with its commitment to combating climate change, the UK government has set ambitious targets to net zero greenhouse gas emissions by 2050, which encompasses areas such as buildings, industry, transportation, and agriculture [2, 3]. In 2019, the Hull City Council declared itself to be a leading carbon-neutral city by achieving net zero emissions by 2030, achieving carbon neutrality 20 years earlier than the UK target and setting up a carbon-neutral model for other cities and countries [4]. In the next ten years, the Hull City Council, in collaboration with its partners, will strive towards changing national policies and additional funding to overcome the big challenge. Especially in the heating sector, there is about 1340 GWh of domestic gas consumption and 1010 GWh of non-domestic gas consumption in heating and industrial processes, whose decarbonization step is identified as the most highly effective carbon-saving and effective measure in delivering carbon reduction [4]. The Hull City Council is exploring more energy-efficient and environmentally friendly options to accelerate heating decarbonization, such as solar collector (SC) and heat pump (HP) heating systems, which are highlighted to further develop for wider applications in the future.

The SC heating systems can directly convert solar energy into heat energy with a simple structure and small energy consumption, which are widely adopted in different buildings [5]. However, the high dependence on solar radiation results in a mismatch between the heating capacity of SC heating systems and the heat load of buildings. The HP heating system extracting stable heat energy from low temperature ambient by consuming electricity, has a high coefficient of performance (COP) over 1 in building heating applications, which is the ideal complementary of the SC heating systems. Therefore, a solar-assisted heat pump heating system (SAHP) is proposed [6, 7] to overcome the deployment challenges of the SC heating system and further reduce the energy consumption of HP, which is an attractive low-carbon energy-saving heating technology [8]. The SAHP harnesses renewable solar radiation as heat for space heating or as a heat source of the HP unit, eventually shorting the running period or increasing the heating performance of the HP unit. Furthermore, the HP unit keeps heat supplying in low radiation period, supplementing the absence of the SC unit. Based on the connection manner between the SC and HP, the SAHP can be mainly classified into three categories, which are series-connected SAHP, parallel-connected SAHP and hybrid-connected SAHP.

The series-connected SAHP utilizes solar energy collected by the SC as the heat source of HP to produce high-temperature water for space heating, and thus has better heat source temperature and preferable heating performance in cold climate applications. Cai et al [9] proposed a novel air source hybrid solar-assisted heat pump which was equipped with a solar-collector evaporator of 4.2 m^2 in a series connection. The simulation results indicated the novel SAHP achieved a higher COP of 3.22 compared to air source heat pump. Tzivanidis et al [10] theoretically investigated the performance of series-connected SAHP and indicated it achieved 47.5% bill savings compared to air source heat pump. However, the series-connected SAHP heavily relies on solar radiation conditions and thus impairs its deployment.

The parallel-connected SAHP, which integrated the heat release coil of SC and the condenser of HP into the same heat storage tank, can generate hot water in different modes. It effectively utilizes the combination of SC and HP during the sunny period and keeps high-efficiency space heating by the separate HP unit in periods of low solar radiation, thus overcoming the operation issue of series-connected SAHP. Jiang et al. [11] designed a novel triangular solar-air collector assisted air source heat pump and proved that it achieved a 64.4% average COP promotion compared to air source heat pump by automatically switching optimal heating mode among preheating to parallel as solar radiation changed.

The hybrid-connected SAHP, of which the SC unit can deliver the solar heat energy to the storage tank or an additional heat exchanger of the HP unit, enables switching between series and parallel connection. Huan et al. [12] proposed a hybrid-connected SAHP system equipped with an automatic type-switching control strategy. The investigation indicated that the serial type performed higher COP than the parallel type in winter but was overtaken by the parallel type during the summer and transition seasons. The hybrid-connected SAHP switched the connection type according to the ambient conditions and eventually achieved the best annual average COP of 5.7, while the annual average COP of serial and parallel-connected SAHP were 3.3 and 4.3, respectively.

Although the hybrid-connected SAHP successfully obtains the advantages of the series-connected SAHP and parallel-connected SAHP, creating a flexible and long-term efficient system, it requires a complex system structure and control strategy due to the variable operation types, which results in the unreliability and high initial cost in practical application. Yang et al. [13] theoretically investigated the three different kinds of SAHP by comparing their energetic and economic performance in London weather conditions. The results discovered that the series-connected SAHP with the largest area of solar collectors and storage tanks could achieve the highest yearly seasonal performance factor of 5.5, but it resulted in the longest payback period of 22.1 years because of the highest initial investment. The parallel-connected SAHP performed a poorer COP of 4.4 but had the shortest payback period of 5.6 years, while the hybrid-connected SAHP obtained a COP of 4.5 but dramatically increased the payback period to 7.2 years.

The parallel-connected SAHP has the highest application potential by comprehensively considering the energetic and economic performance in practical building heating. However, the water temperature of the SC in parallel-connected SAHP is higher than that in the series-connected SAHP, causing a larger heat loss and poorer solar thermal efficiency for the whole system. In addition, the HP unit of parallel-connected SAHP extracts heat from a single source, i.e., the low-temperature outdoor air. Its heating performances are highly reliant on outdoor temperature, of which heating capacity will dramatically decline as outdoor temperature drops, causing deteriorative COP and high power consumption of the system when the building heat load ascends. In addition, the HP's evaporator will meet frequent frosting when the outdoor air temperature is below 5 °C [14] and thus trigger the power-consuming defrosting process. As a result, the parallel-connected SAHP reaches poor seasonal efficiency and does not have wide deployment in practice. Furthermore, most of the novel SAHP technologies were proposed and investigated in theoretical or laboratory conditions so far and thus lacked practical deployment results.

Aiming to tackle these challenges of parallel-connected SAHP, a low-carbon solar-assisted multi-source heat pump heating system (LSMHS) is proposed in the paper, which consists of novel multi-throughout-flowing solar collector (MFSC) arrays and a two-stage heat recovery heat pump (THRHP). The proposed MFSC array is first-of-its-kind. It is the first time that copper tube solar collectors are connected using a multi-throughout-flowing approach that can perform good solar thermal efficiency in high water temperature conditions, fitting with the operation conditions of parallel-connected SAHP. Furthermore, the THRHP extracts exhaust air from the building as an additional heat source for the system, overcoming the deterioration of the heating performance and frequent frosting problems in cold ambiences. The THRHP has been tested and optimized in the laboratory [15] but has yet to be demonstrated in an operational environment. To close the research gaps, the novel MFSC arrays were integrated with the THRHP to develop the innovative LSMHS prototype, which was installed in the Hull Central Library for a long-term practical application. Based on the practical results, the performances of the novel MFSC array are first discussed. By integrating the advantages of the MFSC with THRHP, the operation modes and heating performances of the LSMHS in different weather conditions are then analyzed to discover insights into the LSMHS working characteristics in public building heating. Thereafter, the eco-economic performances of the system are further studied to reveal the application potential of the LSMHS. This investigation provides valuable data on the first practical application of the LSMHS and thus discloses its feasibility and advantages, which contribute to accelerating the deployment of low-carbon building heating systems and achieving ambitious carbon-neutral targets.

2. The structure of the novel low-carbon solar-assisted multi-source heat pump heating system

2.1. The multi-throughout flowing solar collector array of the novel system

Traditional copper tube solar collectors meet application problems when many collectors connect in a one-to-one connection method. Figure 1 (a) shows the schematic of the most common solar collector in the market. It connects copper tubes in parallel to one inlet head tube and one outlet head tube, and forms a collector array in the one-to-one connection approach. The water flows through the copper tubes in uneven distribution and low flow rate, which caused the low heat transfer coefficient in some tubes as well as the poor solar thermal efficiency for the parallel solar collector array. Figure 1 (b) further shows another commercial solar collector that connects the copper tubes in series by a large number of U-turns, forming the series solar collector array in the one-to-one connection approach. The total flowing resistance of the series solar collector array is higher than the parallel solar collector array because of the large water flow rate and the total number of U-turns, which causes the high-power consumption of circulation pump and blocks its scalable application.

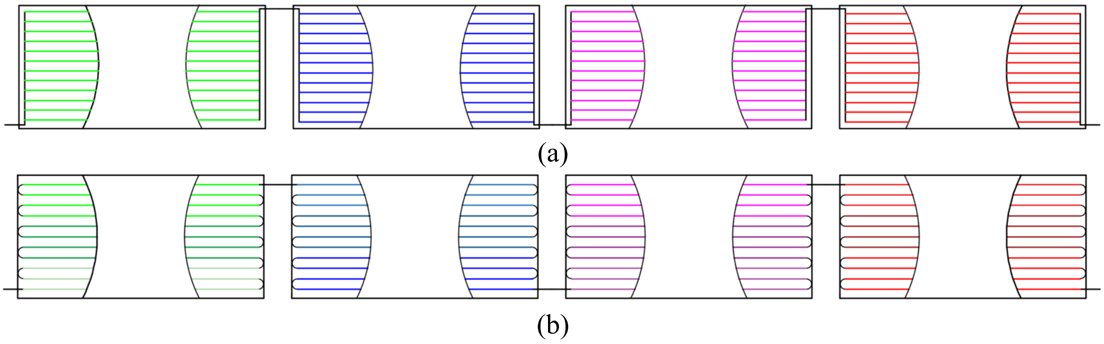

Figure 1. Traditional solar collector arrays (a) Parallel solar collector array (b) Series solar collector array

Figure 2 shows the novel MFSC array developed for the first time in this paper. The designed MFSC consists of 12 copper tubes in 4 passes with 4 inlets and 4 outlets, of which structure details are shown in Figure 2 (a). Each set of inlet/outlet head tubes contains 3 copper tubes, forming a single pass. The corresponding passes of the four MFSCs are connected in series and then each pass is linked together, becoming the multi-throughout-flowing solar collector array, as shown in Figure 2 (b) and (c). The working fluid flows through the first pass and then turns into the second pass, reciprocating around the whole array several times, which increases the water flow rate and achieves much more even distribution in each copper tube when compared to the parallel solar collector array. In addition, compared to the series solar collector array, the MFSC array significantly reduces the U-turns number and thus theoretically has lower flowing resistance, which is another important promotion for practical application.

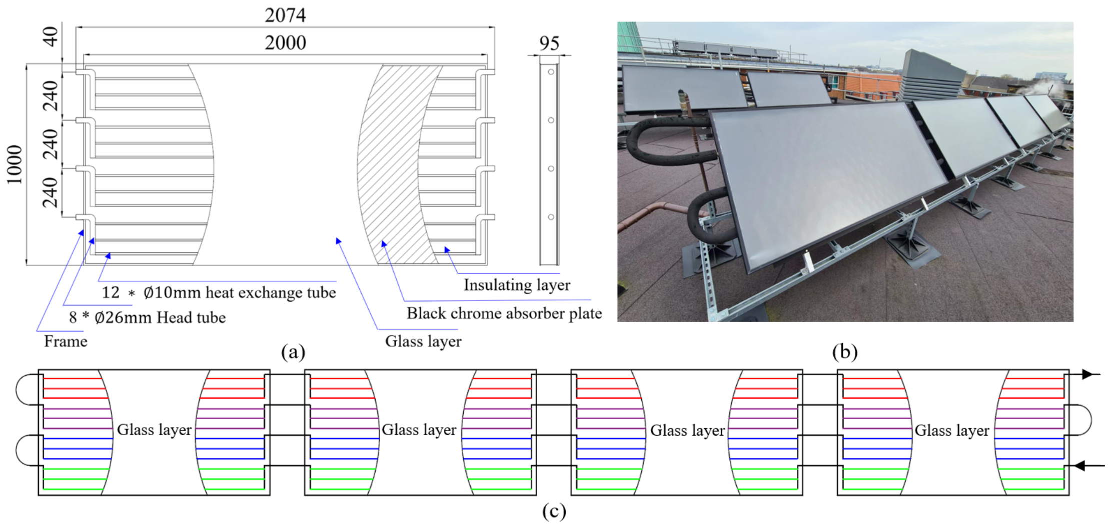

Figure 2. The novel MFSC array (a) Structure details of the MFSC (b) Practical MFSC array (c) Connection diagram of the MFSC array

2.2. The two-stage heat recovery heat pump of the novel system

In practical applications of parallel-connected SAHP, the heating demand of buildings increases quickly as outdoor temperature declines, while the heating capacity and COP of the HP unit decrease dramatically. Besides the contradiction between the increasing heating demand and decreasing heating capacity, most buildings have ventilation requirements, where the exhaust air has a great amount of waste heat. However, the waste heat is either ejected into the atmosphere or partially recovered by using mechanical ventilation heat recovery devices with additional energy consumption. To overcome these application challenges of parallel-connected SAHP, a THRHP is applied in the novel LSMHS.

As Figure 3 depicts, the THRHP is composed of medium-pressure evaporator (ME), low-pressure evaporator (LE), condenser, economizer, vapor injection compressor, exhaust air fan and discharge air fan. On the airflow side, the exhaust air is extracted as a second heat source by the THRHP and flows through the ME. The exhaust air is first recovered by the ME and then mixed with the outdoor air after the ME. Afterwards, the mixed air flows through the LE, acting as the heat source of the LE for the second stage of heat recovery. Through the two-stage heat recovery, the discharge air reaches a lower temperature than the ambient when it leaves the THRHP, thus achieving over 100% exhaust waste heat recovery. Besides, the warm second heat source improves the evaporation temperatures and thus promotes the heat performance of THRHP. The warm exhaust air can be further used to retard frosting and efficient defrosting for the THRHP in cold weather. On the refrigerant side, the discharged refrigerant is first cooled down in the condenser and then divided into three streams. One stream is evaporated in the ME after throttle. The second stream flows through the economizer and cools the third stream. After the economizer, the third is throttled and evaporated in the LE. After that, the three streams flow back to the vapor injection compressor. The vapor injection compressor ejects the medium-pressure refrigerant from the ME and economizer to cool down the compressed refrigerant coming from the LE, therefore reducing the discharge temperature as well as the total power consumption of THRHP. At the same time, the refrigerant flow rate in the condenser is therefore enlarged owing to the additional injected medium-pressure refrigerant, thus increasing the heat capacity as well as COP at last. Figure 4 shows the practical structure of the proposed THRHP prototype. Before being applied to the practical building, the THRHP prototype was tested and optimized to the best performance in conditions of low outdoor temperature and high water outlet temperature in the environmental laboratory, which achieved synergistic promotion by integrating the abilities of heating, ventilation and heat recovery [15]. In addition, owing to the high water temperature output, the THRHP was suitable to directly replace the gas boiler by adapting to its original heating terminals without additional retrofitting.

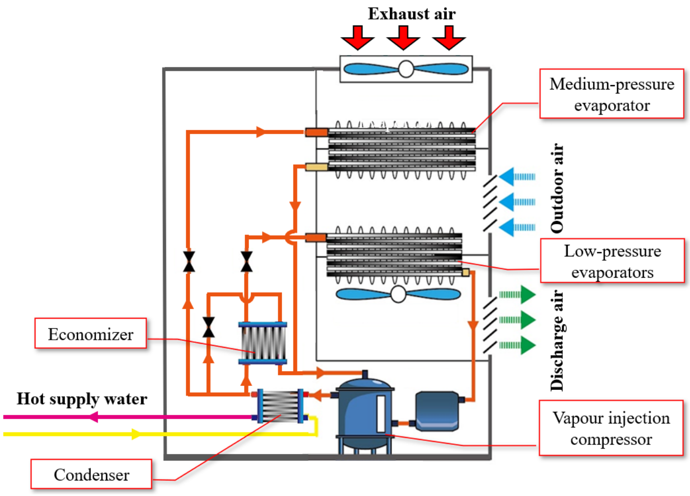

Figure 3. Schematic diagram of the THRHP

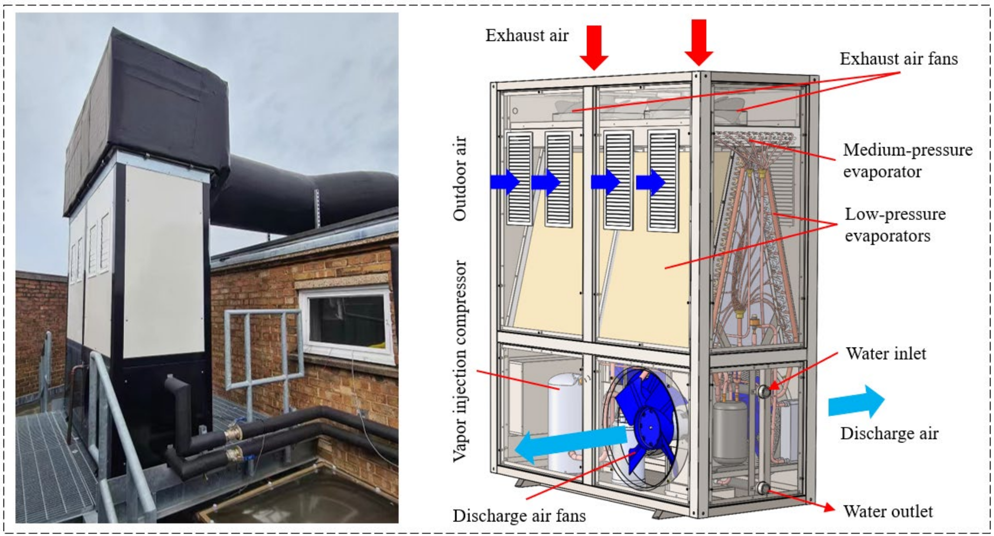

Figure 4. Practical structure of the THRHP

2.3. The structure of the novel low-carbon solar-assisted multi-source heat pump heating system

Figure 5 shows the pipe and instruction diagram of the LSMHS. The MFSC arrays and THRHP are connected in parallel to the heat storage tanks, and then the tanks link to the fan coil terminals of a workshop. The THRHP extracts exhaust air through the air duct and keeps the fresh air flowing into the workshop, while the exhaust air flow rate is controlled by the damper. As a result, the THRHP gratifies the ventilation requirements of users and simultaneously recovers the waste heat from exhaust air, which can improve the heating capacity and reduce power consumption. The hot water produced by the THRHP flows into the tanks from the top inlet and returns to the THRHP through the bottom outlet of the tanks, forming the HP circuit. The several MFSC arrays parallelly connect to the main tubes and then link to the immersive heat exchangers of the tanks, becoming the SC circuit. The solar heat collected by the MFSC arrays is released to the water tanks by the immersive heat exchangers and stored for building heating. Thereafter, 8 original fan coil terminals warm the workshop by delivering the hot water from the top of the tanks and then returning cold water to the bottom of the tanks, which is called FC circuit. In this connection method, the produced hot water from the HP circuit can be delivered to the FC circuit as fast as the THRHP starts operation, ensuring the quick response time of the workshop heat load. Also, the SC circuit can operate at a relatively lower water temperature at the bottom of the tanks.

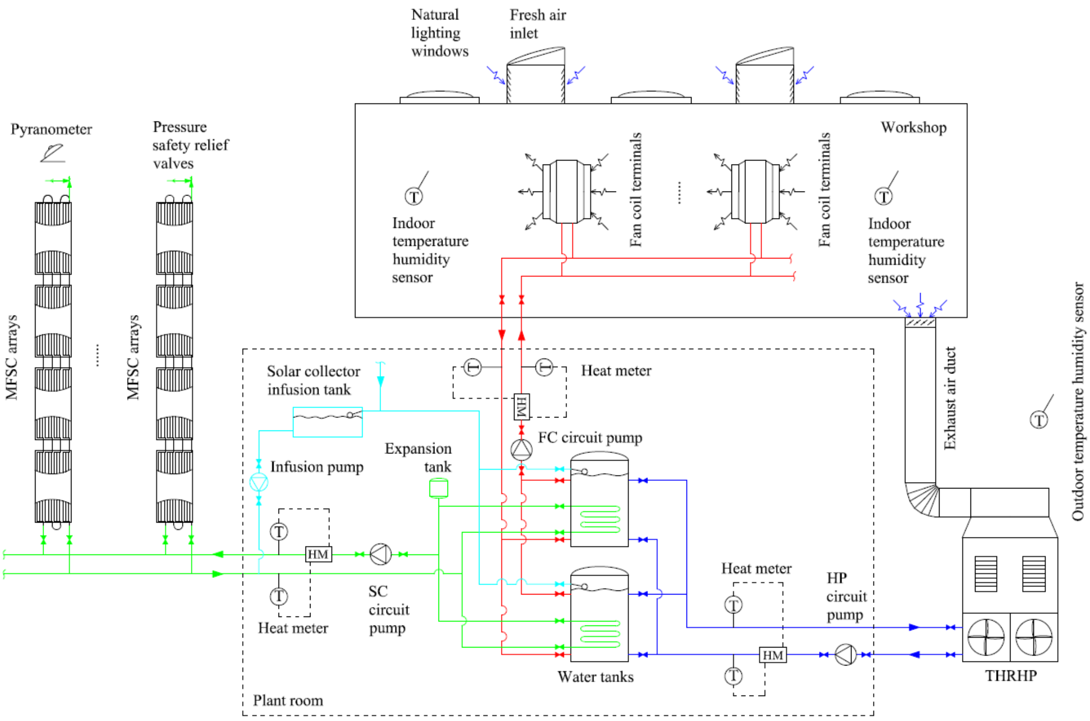

Figure 5. Pipe and instruction diagram of the LSMHS

Figure 6 (a) to (c) depict the practical distribution of every component of the LSMHS in the Hull Central Library. From Figure 6 (a), the SC circuit has 8 MFSC arrays in parallel connection, forming a 64 m^2 solar collector field. They are distributed southwards in parallel on the roof of the Hull Central Library. Figure 6 (b) shows that the THRHP is installed on the roof of the library adjacent to the plant room, while the exhaust air duct runs along the exterior wall of the library from the top of the THRHP to the workshop. Figure 6 (c) depicts that the indoor space is heated by 8 original fan coil terminals, while the indoor ventilation is conducted through the exhaust air duct in the lower right corner of the workshop. The SC circuit, the HP circuit and the FC circuit are parallelly connected to the two 600 L water tanks in the plant room.

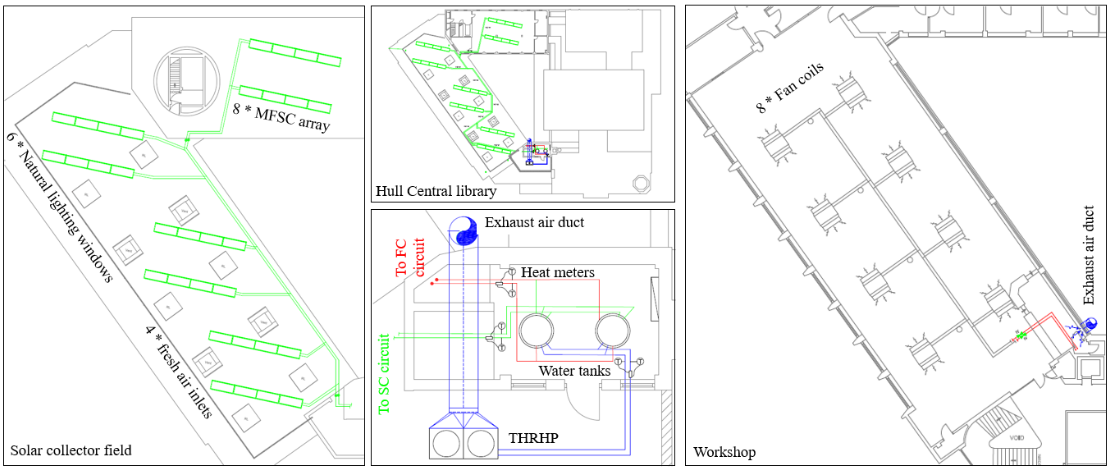

(a) (b) (c)

Figure 6. Practical construction of the LSMHS on the Hull Central Library (a) the SC circuit (b) the HP circuit (c) the FC circuit

Figure 7 presents the practical structure of the LSMHS, and the component details of the system are listed in Table 1. The total area of the MFSC arrays is 64 m^2, which is determined by the roof area. The exhaust airflow rate of LSMHS is adjusted to 0.9 m^3/h following the ASHRAE [16]. The designed heating capacity of THRHP is 32 kW under conditions of 55 °C water outlet temperature and 0 °C outdoor air temperature. All these components are controlled by the operation strategy of a self-built control box in the plant room. First, the whole system has a priority operation period control scheme which is adjustable according to the actual staff's working time and environmental conditions. Behind the priority operation period control, the THRHP runs according to its water outlet temperature, which starts running when the water outlet temperature is below the lower limit of 50 °C and stops working when the water outlet temperature reaches the upper limit of 60 °C. Regarding the SC circuit, its circulation pump is controlled by the temperature difference between a reference temperature on the highest point of the SC circuit and the water tank temperature. When the reference temperature exceeds the water tank temperature by 5 °C, the control box treats the solar radiation as sufficient and turns on the SC circulation pump. Otherwise, the SC circulation pump is stopped. Furthermore, the FC circuit depends on the indoor temperature. When the indoor temperature is lower than 18 °C, the FC water pump starts running. When the indoor temperature is higher than 24 °C, the FC water pump stops running.

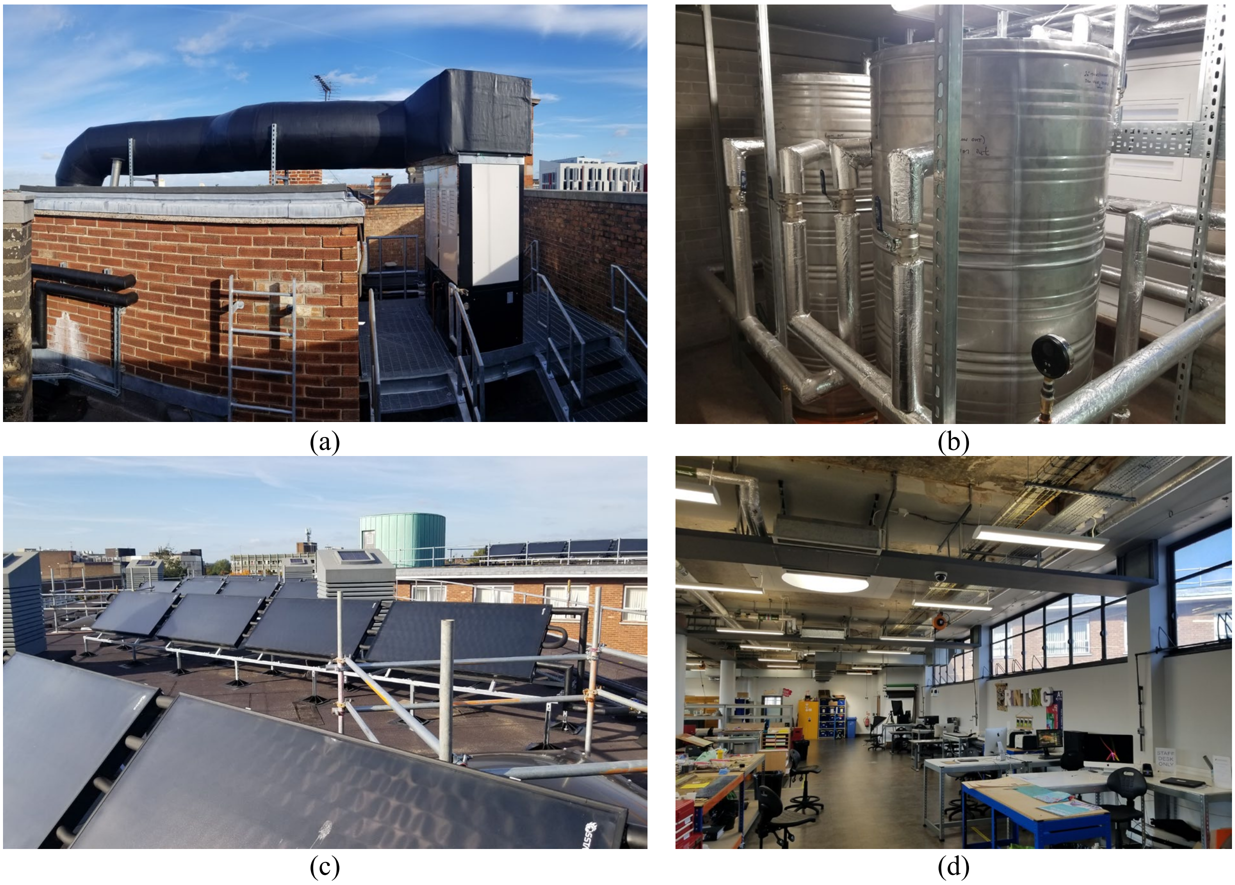

Figure 7. Real-life installation of the LSMHS at the Hull Central Library (a) the THRHP (b) the heat storage water tanks (c) the MFSC arrays (d) the fan coil terminals and the workshop

Table 1. Component details of the LSMHS

Main components	Parameters	Specifications
THRHP	Model	DKRS-10 (13X)
	Size	2150mm * 1800mm * 750mm
MFSC	Size	2000mm * 1000 mm * 95mm * 32
Heat storage water tank	Model	FS-HEDX-2020SX000
	Volume	600L * 2
Exhaust air duct	Size	Ø 750mm
Exhaust air damper	Size	770mm * 770mm
HP circuit water pump	Model	Grundfos Magna3
SC circuit water pump	Model	Wilo Economy MHI 205
FC circuit water pump	Model	Grundfos Alpha3

Figure 8 depicts the remote control and monitoring subsystem of LSMHS, which implements real-time data monitoring and system adjusting, and thus delivers the best system performance. Figure 8 (a) shows the local data collection devices of the subsystem, which include an MBUS data logger, an RS485 converter, an Agilent data logger, a 5G Wi-Fi module, and a micro desktop computer. After collecting and organizing the data from different sensors, the local data collection computer uploads data to the cloud services and displays it in the user interface in real time. The user can remotely monitor the LSMHS and control every component through the remote control and monitoring interface (see Figure 8 (b)). Therefore, the priority operation period of the whole system, and the upper and lower temperature limits of the HP circuit and FC circuit are all adjustable according to the practical requirements. Based on automatic control, the MFSC arrays collect solar thermal energy during sunny periods, and the THRHP produce heat by absorbing heat from the exhaust air and outdoor air during cloudy periods. The control scheme will maximize the renewable solar energy utilization of MFSC arrays and minimize the operational hours as well as energy consumption of the THRHP, achieving the best bill-saving and carbon reduction performance in the long-term operation of the LSMHS.

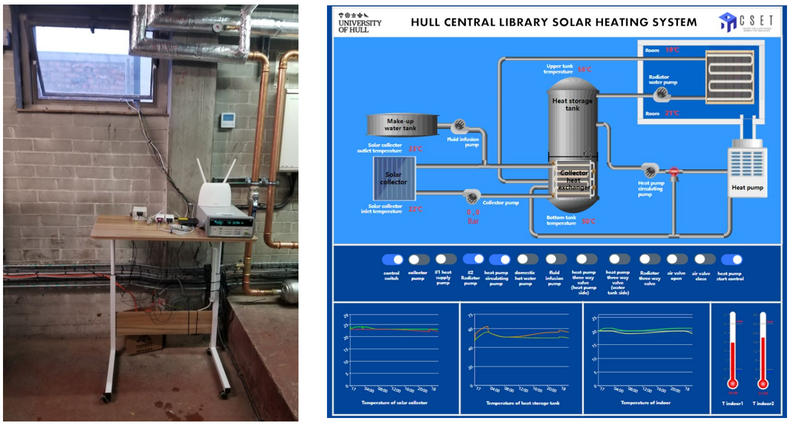

(a) (b)

Figure 8. The remote control and monitoring subsystem of the LSMHS (a) Local data collection devices (b) Remote control and monitoring interface

3. System evaluations of the LSMHS

The heating system applied industrial sensors and equipment to conduct data measurements and collections. As shown in Figure 6(a), the heating capacity of the THRHP, the heat collection of the MFSC arrays, and the heat supply of fan coil terminals are measured by three industrial heat meters, respectively. The power consumption of water pumps is measured by the built-in power meters, while the power consumption of THRHP was measured by current transformers. The outdoor and indoor temperature and humidity are measured by standard temperature humidity sensors, and the solar radiation is measured by a pyranometer. The model information and accuracy of each sensor are summarized in Table 2. The essential environmental parameters and evaluation factors of the LSMHS are concluded below.

The average outdoor and indoor temperatures can be calculated by:

$$\bar{T}_{\mathrm{out}} = \frac{\sum T_{\mathrm{out,i}}}{\sum i} \tag{1}$$

$$\bar{T}_{\mathrm{in}} = \frac{\sum T_{\mathrm{in,i}}}{\sum i} \tag{2}$$

where $\bar{T}_{\mathrm{out}}$ and $\bar{T}_{\mathrm{in}}$ are the average outdoor and indoor temperatures during staff's working time, respectively, $T_{\mathrm{out,i}}$ and $T_{\mathrm{in,i}}$ are real-time outdoor and indoor temperatures, respectively, where i is the measurement interval of the monitoring subsystem. All demonstration data are measured in minutes and displayed in real-time.

The average outlet and inlet water temperature of the three circuits during their corresponding operation period can be calculated by:

$$\bar{T}_{\mathrm{w,outlet}} = \frac{\sum T_{\mathrm{w,outlet,i}}}{\sum i} \tag{3}$$

$$\bar{T}_{\mathrm{w,inlet}} = \frac{\sum T_{\mathrm{w,inlet,i}}}{\sum i} \tag{4}$$

where $T_{\mathrm{w,outlet,i}}$ and $T_{\mathrm{w,inlet,i}}$ are the real-time water outlet and inlet temperature of the corresponding circuit, respectively.

The average solar radiation is expressed as:

$$\bar{R} = \frac{\sum R_{\mathrm{i}}}{\sum i} \tag{5}$$

where $\bar{R}$ is the average solar radiation during the staff's working time, R_{i} is real-time solar radiation.

The real-time heating capacity of the THRHP, the heat collection of the MFSC arrays, and the heat supply of fan coil terminals therefore are evaluated by:

$$Q_{\mathrm{THRHP,i}} = c\rho\dot{v}_{\mathrm{i,THRHP}}\left(T_{\mathrm{THRHP,w,outlet,i}} - T_{\mathrm{THRHP,w,inlet,i}}\right) \tag{6}$$

$$Q_{\mathrm{SC,i}} = c\rho\dot{v}_{\mathrm{i,sc}}\left(T_{\mathrm{SC,w,outlet,i}} - T_{\mathrm{SC,w,inlet,i}}\right) \tag{7}$$

$$Q_{\mathrm{FC,i}} = c\rho\dot{v}_{\mathrm{i,FC}}\left(T_{\mathrm{FC,w,inlet,i}} - T_{\mathrm{FC,w,outlet,i}}\right) \tag{8}$$

where c is the special heating capacity of water, ρ is the density of water, and $\dot{v}_i$ are corresponding water volume flow rates of the HP circuit, SC circuit and FC circuit, which are respectively adjusted to around 5.0 m^3/h, 4.8 m^3/h and 2.5 m^3/h in the practical application.

Respecting the SC circuit, the real-time overall thermal efficiency of the MFSC arrays is evaluated by:

$$\partial_{\mathrm{SC,i}} = \frac{Q_{\mathrm{SC,i}}}{64 * R_{\mathrm{i}}} \tag{9}$$

Furthermore, solar thermal efficiency can be expressed as the relationship between outdoor temperature, water temperature, and solar radiation, which is called collector efficiency normalization curve and can be regressed according to Ref [17] and [18]:

$$\partial_{\mathrm{SC,i}} = \partial_{\mathrm{SC,0}} - a_1 T_{\mathrm{m}} - a_2 {T_{\mathrm{m}}}^2 R_{\mathrm{i}} \tag{10}$$

$$T_{\mathrm{m}} = \frac{\frac{\left(T_{\mathrm{SC,w,outlet,i}} + T_{\mathrm{SC,w,inlet,i}}\right)}{2} - T_{\mathrm{out,i}}}{R_{\mathrm{i}}} \tag{11}$$

where $\partial_{\mathrm{SC,0}}$ is optical efficiency, a_1 is thermal losses linear coefficient, a_2 is the thermal losses quadratic coefficient, and T_{m} is normalization temperature of solar collector.

The real-time power consumption of THRHP is calculated by:

$$W_{\mathrm{THRHP,i}} = U\left(I_{1,\mathrm{i}} + I_{2,\mathrm{i}} + I_{3,\mathrm{i}}\right)\theta_{\mathrm{i}} \tag{12}$$

where U is the voltage of THRHP which is the standard grid voltage of the UK, $I_{1,\mathrm{i}}$, $I_{2,\mathrm{i}}$, $I_{3,\mathrm{i}}$ are the line current of each phase of THIHP, and θ_{i} is the power factor of THRHP.

Thereafter, the real-time COP of the system is expressed as:

$$COP_{\mathrm{sys},i} = \frac{Q_{\mathrm{THRHP,i}} + Q_{\mathrm{SC,i}}}{W_{\mathrm{THRHP,i}} + W_{\mathrm{HP,pump,i}} + W_{\mathrm{SC,pump,i}} + W_{\mathrm{FC,pump,i}}} \tag{13}$$

where the sum of $Q_{\mathrm{THRHP,i}}$ and $Q_{\mathrm{SC,i}}$ is real-time heating capacity of the system, $W_{\mathrm{THRHP,i}}$ is real-time power consumption of the THRHP, and $W_{\mathrm{HP,pump,i}}$, $W_{\mathrm{SC,pump,i}}$, and $W_{\mathrm{FC,pump,i}}$ are real-time pump power consumption of water pumps of the HP circuit, SC circuit and FC circuit, respectively. The power consumption of all components adds up to the real-time power consumption of the system.

In the long-term operation of LSMHS, the total heat generation (*HG*) of THRHP, the total heat collection (*HC*) of the MFSC arrays, and the total heat supply (*HS*) of the fan coil terminals are evaluated by:

$$HG = \sum i \, Q_{\mathrm{THRHP,i}} \tag{14}$$

$$HC = \sum i \, Q_{\mathrm{SC,i}} \tag{15}$$

$$HS = \sum i \, Q_{\mathrm{FC,i}} \tag{16}$$

As a result, the total heat production (*HD*) of the LSMHS is expressed as:

$$HD = HG + HC \tag{17}$$

Besides, the total energy consumption of the LSMHS is calculated by:

$$E = \sum i \left(W_{\mathrm{THRHP,i}} + W_{\mathrm{HP,pump,i}} + W_{\mathrm{SC,pump,i}} + W_{\mathrm{FC,pump,i}}\right) \tag{18}$$

Therefore, the average COP of the system can be expressed as the ratio of total heat production to total energy consumption, which is shown below:

$$COP_{\mathrm{sys,ave}} = \frac{HD}{E} \tag{19}$$

The uncertainties of the evaluation factories are accumulated from the accuracy of sensors according to Ref [19], which are calculated as:

$$y = f(x_1, x_2, x_3, \cdots\cdots, x_n) \quad (20)$$

$$U_y = \left[\left(\frac{dy}{dx_1} U_{x_1} \right)^2 + \left(\frac{dy}{dx_2} U_{x_2} \right)^2 + \left(\frac{dy}{dx_3} U_{x_3} \right)^2 + \cdots\cdots + \left(\frac{dy}{dx_n} U_{x_n} \right)^2 \right]^{0.5} \quad (21)$$

where y is a function of $x_1, x_2, x_3, \cdots\cdots, x_n$, U_i is the uncertainties of parameter i. As a result, the uncertainties of heating capacity, power consumption and *COP* are 9.52%, 12.91% and 13.06%, respectively.

Table 2. The accuracy of measurement sensors

Sensors	Model	Parameters	Accuracy
Heat meter	Multical 403	Water temperature (ºC)	±0.1 ºC
		Water flow rate (m^3/h)	±1.95%
Temperature humidity sensor	DL-10	Air Temperature (ºC)	±0.4%
		Air Humidity (%)	±3%
Pyranometer	HQTBQSV240C	Solar radiation (W/m^2)	±2%
Current transformer	RS PRO 1718764	Current (A)	±1%
Power meter of water pump	Grundfos Alpha3	Power consumption (W)	±5%

4. Results and discussions

The practical data of the MFSC is analyzed to reveal its performance in large-scale deployment at first. Thereafter, the daily and monthly performances of the LSMHS are discussed to give the most insights into the operating modes, heating performance and eco-economic performance of the system in different weather conditions.

4.1. Practical performance of the MFSC

Figure 6 illustrates the performance of the MFSC arrays on 3 typical days, which are 21st to 23rd Mar 2022. The outdoor temperature increased from the lowest point around 7:00 every day as the sunrise, and then peaked at the highest temperature at midday, ranging from -0.92 ºC to 28.89 ºC throughout the days. The solar radiation was strong and abundant which respectively peaked at 918.42 W/m^2, 782.33 W/m^2 and 857.96 W/m^2 in the three days. In such operation conditions, the MFSC arrays started working around 9:00 every day and raised the water temperature as the solar radiation and outdoor temperature increased, reaching a maximum water outlet temperature of 74.82 ºC and averaging at 64.57 ºC, and thus, the practical normalized temperature of the SC circuit ranged from 0.052 K/(W/m^2) to 0.163 K/(W/m^2). The application results indicated that the MFSC arrays mainly worked at conditions of high water temperatures and high normalized temperatures when applied in the LSMHS.

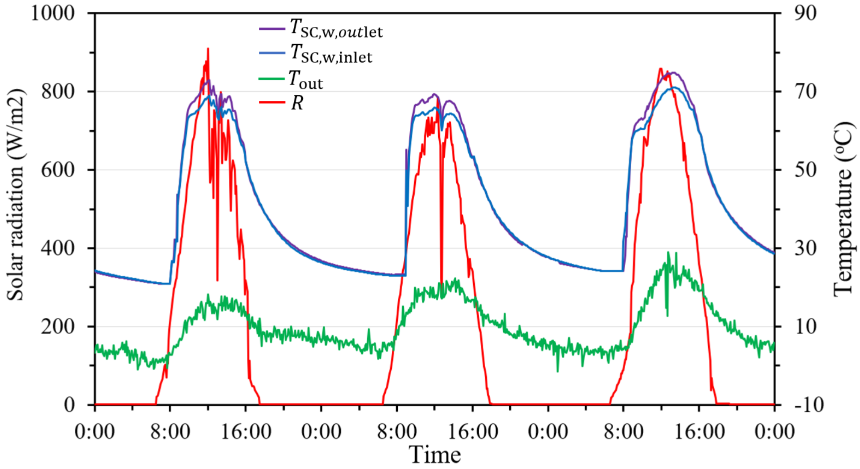

Figure 9. Typical operation days of MFSC arrays

Figure 10 depicts the collector performances of the novel MFSC arrays. The heating capacity of MFSC arrays rose with the solar radiation every day and was able to reach the maximum heating capacity of 22900 W, 19300 W and 23800 W on 21st, 22nd, and 23rd Mar, i.e. 2862.5 W, 2412.5 W and 2975.0 W per array, respectively. Thus, the solar thermal efficiency of MFSC changed with solar radiation, which was up to 46.74% on 23rd Mar when the normalized temperature was 0.066 K/(W/m^2).

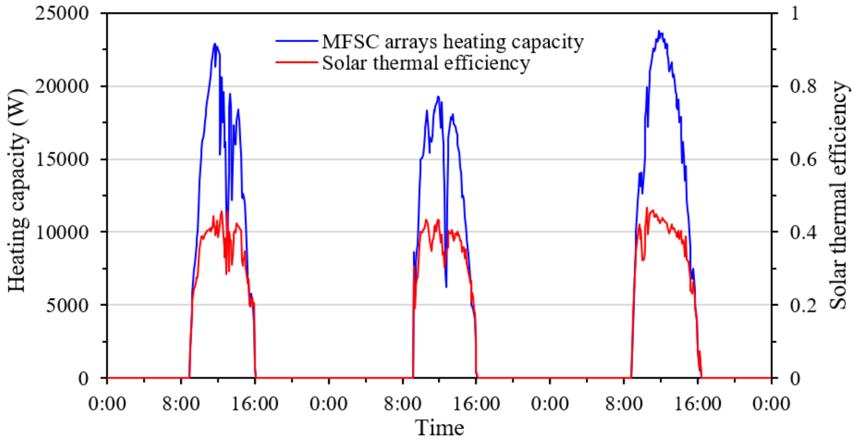

Figure 10. Heating performance of the MFSC arrays

Figure 11 summarizes all application results of the MFSC arrays to further reflect its practical performance. The MFSC arrays mainly worked at high normalized temperature conditions, ranging from 0.0479 to 0.1382 W/m^2/K, which was higher than traditional solar collectors. The MFSC arrays achieved a maximum heating capacity of 24400 W and its highest solar thermal efficiency was 48.97% in practice. The solar thermal efficiency of the MFSC arrays was in decreasing trend when the normalized temperature rose. According to Ref [17, 18], the collector efficiency normalization curve of the MFSC arrays is regressed from the practical testing results, of which the optical efficiency is 0.6488, the thermal losses linear coefficient is 2.9874 W/m^2/K, and the thermal losses quadratic coefficient is 0.0256 W/m^2/K^2, respectively. Thus, the solar thermal efficiency can be expressed in Eq. (22). The regressed optical efficiency of the MFSC arrays is relatively lower than the solar collector of Ref [20] because most of the data of MFSC arrays were achieved at high water temperatures (>55 °C) in the practical application.

$$\partial_{\mathrm{MFSC,i}} = 0.6488 - 2.9874T_{\mathrm{m,i}} - 0.0256{T_{\mathrm{m,i}}}^2R_{\mathrm{i}} \quad (22)$$

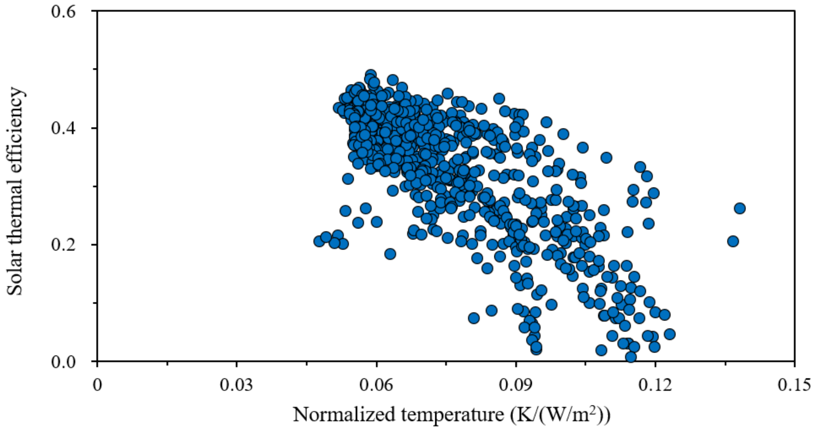

Figure 11. Practical performance of the MFSC arrays

4.2. Operation characteristics of the LSMHS

The demonstration LSMHS was operated for a long period between Jan and Mar 2022 which contained practical results from a total of 68 days. The practical heating performances of the LSMHS were concluded first, and operational modes of the LSMHS are analyzed in detail through the most representative days of the three months, giving deep insights into the operation characteristics of LSMHS under different environmental conditions.

4.2.1 Practical operation of the LSMHS in Jan

Figure 12 shows the Jan operation performances of the LSMHS. As shown in Figure 12 (a), the daily system heat production of the LSMHS ranged from 130.94 kWh to 399.62 kWh. The fluctuation of daily system heat production was due to several influences, which not only changed with ambient conditions, such as outdoor temperature and solar radiation, but also were severely affected by human activities. For instance, the demonstration workshop was a business workshop that could be rented by the public for events, so, the internal heat gain from humans and devices significantly increased in some days, leading to obvious declines in the workshop's heat load as well as daily system heat production. On the contrary, the building heat load increased with other human activities, such as natural ventilation when opening windows, mechanical ventilation when making handcraft, etc. Therefore, the daily system heat production was unpredictable when human activities were included. Furthermore, the daily system energy consumption is illustrated in Figure 12 (b), which was changed uniformly with the daily system heat production, ranging from 68.60 kWh to 191.88 kWh. To clearly analyze the operation modes and performance of the LSMHS in Jan, a most representative experimental day was zoomed in as follows to disclose insights into the practical system operation in Jan.

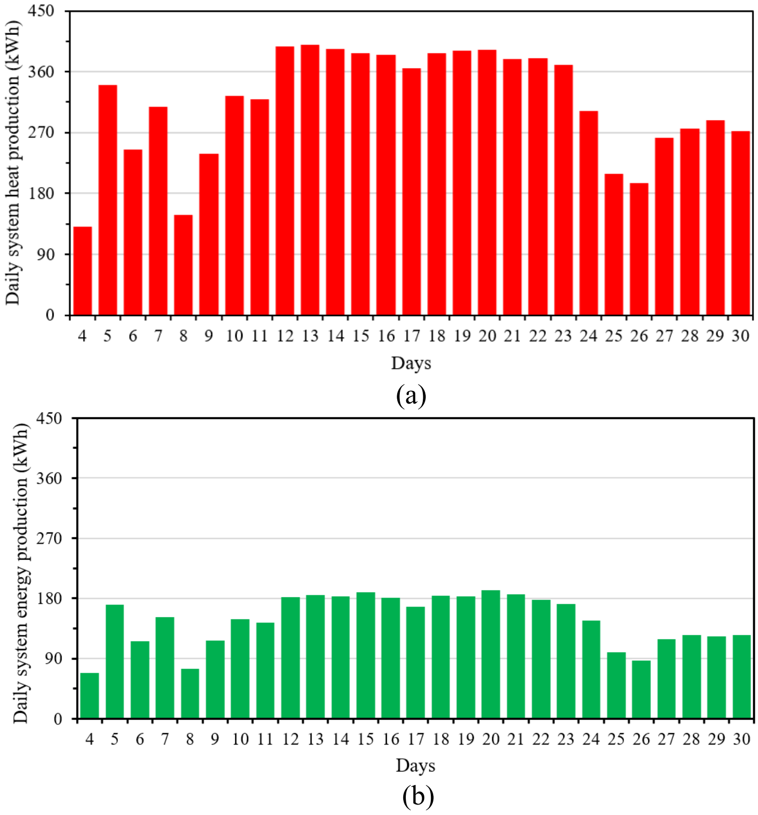

Figure 12. Practical operation reuslts of the LSMHS in Jan (a) System heat production (b) System energy consumption

Figure 13 presents the most typical operation conditions of the LSMHS on a day of Jan. The outdoor temperature was cold while the solar radiation was not abundant. The outdoor temperature was constant between -2.50 °C to 2.50 °C most of the time and raised with solar radiation during the midday. The outdoor temperature peaked at 7.92 °C and the strongest solar radiation was 718.69 W/m^2 on 5th Jan, and thus the daily average outdoor temperature and solar radiation during the working time of the library were only 3.96 °C and 146.33 W/m^2, respectively. Respecting the indoor temperature, it was maintained above 19.0 °C and reached the highest point of 22.0 °C at midday, achieving an average indoor temperature of 20.60 °C. It indicated that the novel LSMHS was able to satisfy the workshop heat load and occupant thermal comfort in the coldest month of Hull.

Furthermore, Figure 13 shows the fluctuation of water temperatures of the main operating circuits, i.e., the HP circuit and the FC circuit. The SC circuit did not work on 5th Jan because the outdoor temperature was too low even though the solar radiation was good in some periods. Thus, the curve of the SC circuit was not shown. The heat demand of the workshop was mainly covered by the THRHP in the cold Jan, which is called THRHP mode of the LSMHS. The HP circuit outlet temperature rising from 50 °C to 60 °C took 41 to 81 mins, which is named heating period for simplicity. Besides, the HP circuit outlet temperature descended from 60 °C to 50 °C was 43 to 48 mins, which is called heat-releasing period. Eventually, the fluctuating HP circuit outlet temperature reached an average value of 57.31 °C, and the FC circuit inlet temperature had an average value of 55.04 °C. Furthermore, the HP inlet and outlet temperatures had several short-term overlaps during the heating period, which was due to the defrosting process stopping the compressor and using the exhaust air to melt the frost of evaporators. These defrosting processes of THRHP only cost around 4 mins and 270.47 W to 307.59 W in the practical application, significantly reducing the defrosting energy consumption.

The practical results indicated that the LSMHS can work well with the library's original fan coil terminals due to the high water temperature output. This characteristic of high water temperature output significantly reduced the retrofitting cost when the LSMHS replaced the traditional gas boiler heating system of the library, which benefits the low-carbon heating deployment.

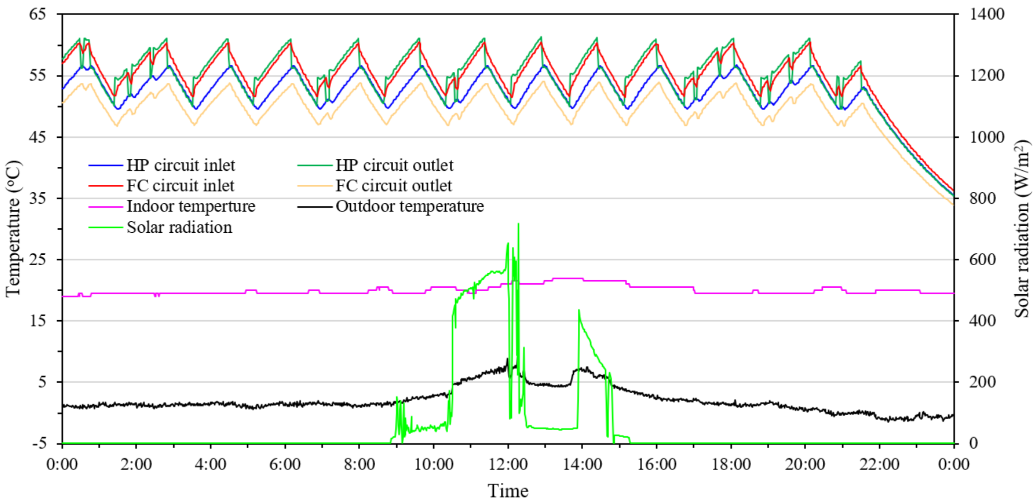

Figure 13. Operation conditions of the LSMHS on 5th Jan 2022

Figure 14 depicts the heating performance of the LSMHS. The system heating capacity ranged from 26800W to 32300 W. Since the system heating capacity was fully contributed by the THRHP, it should slightly increase with the HP circuit water outlet temperature as Ref [15] depicted. However, the higher water temperature caused a larger heat loss on the surface of long connection tubes in practical application, and thus surpassed the small increase of the heating capacity in low outdoor temperatures. Furthermore, the THRHP stopped in the heat-releasing period but the HP circulation water pump kept running to prevent the condenser and pipe frosting in cold ambient. Thus, the system heating capacity is negative in the heat-releasing period due to the heat loss from the exposed surface.

The system heat supply from the FC circuit was always lower than the system heating capacity during the heating period. The surplus heat production was stored in the water tanks during the heating period and then kept the FC circuit running during the heat-releasing period. The system heat supply was around 12000 W to 15000 W when the THRHP stopped, but it quickly increased to around 16000 W to 21000 W when the THRHP operated. The quick response of the system heat supply ability indicated that the connection in water tanks can deliver the high-temperature water produced by THRHP to the fan coil terminals immediately, and thus achieve a quick response to the building heat load.

The power consumption of the system also mainly came from the THRHP, which was raised with the water outlet temperature of THRHP, coinciding with the Ref [15] discovery. Therefore, the power consumption of the novel heating system ranged from 11763 W to 14890 W as the HP circuit outlet temperature rose during the heating period and only had around 114 W from the water pumps during the heat-releasing period.

As a result, the total HD of the LSMHS achieved 340.37 kWh on 5th Jan. The total energy consumption of the system was 170.62 kWh, in which the THRHP contributed 167.89 kWh, while the HP and FC circulation water pump only occupied 2.73 kWh. Eventually, the COP_{sys} diminished with the water outlet temperature due to the increasing power consumption, and so, the COP_{sys} of the LSMHS ranged from 1.72 to 2.48 on 5th Jan.

In summary, the LSMHS only operated THRHP mode in cold weather. The LSMHS achieved an average $COP_{sys,ave}$ of 1.99 when it produced high-temperature water averaging at 57.31 ºC to maintain indoor comfort by absorbing heat from the cold outdoor air of 3.97 ºC and recovering waste heat from the warm exhaust air of 20.60 ºC.

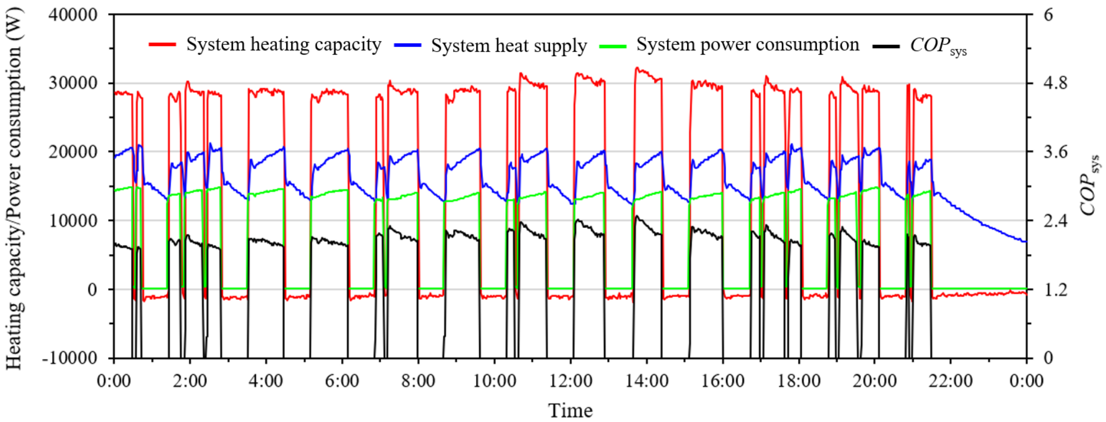

Figure 14. Practical performances of the LSMHS on 5th Jan 2022

4.2.2. Practical operation of the LSMHS in Feb

Figure 15 illustrates the practical operation performance of the LSMHS in Feb. As Figure 15 (a) shows, the daily system heat production in Feb ranged from 172.36 kWh to 384.95 kWh. The days that were not presented were maintenance days when the LSMHS needed to be shut down for a check and adjustment. Furthermore, the change of daily system heat production between the 13th and 21st was mainly attributed to the operation strategy adjustment according to the staff's requirements. Figure 15 (b) depicts the daily system energy consumption of the LSMHS in Feb, which ranged from 68.31 kWh to 178.10 kWh, slightly lower than those in Jan. To further discuss the operation characteristics and performances of the LSMHS in Feb, the most representative day of Feb was further zoomed in and analyzed in detailed. The differences in the operation performance of the LSMHS between Jan and Feb were also discussed in the daily analysis as follows.

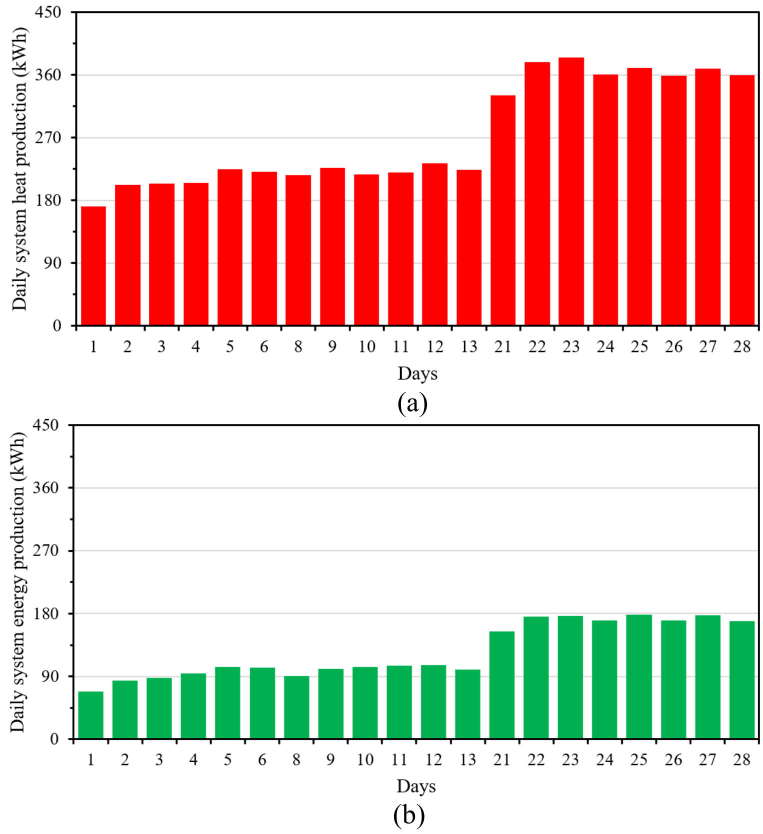

Figure 15. Practical operation results of the LSMHS in Feb (a) System heat production (b) System energy consumption

Figure 16 illustrates the typical operation conditions of LSMHS on a day of Feb. The outdoor temperature in Feb was warmer than that in Jan, which changed between 6.46 ºC and 8.84 ºC. However, the solar radiation in Feb was still poor, eventually achieving an average outdoor temperature of 6.87 ºC and an average solar radiation of 15.49 W/m^2 on 13th Feb. Due to the warmer outdoor temperature, the LSMHS was set to operate from 6:00 to 19:00 on 13th Feb, which was long enough to maintain the indoor temperature during the working time of staff. The indoor temperature increased from 17.22 ºC when the LSMHS started operating and then fluctuated with the change of water temperature during the working time, ranging between 19.24 ºC and 20.44 ºC, with an average of 19.90 ºC.

Besides, the HP water outlet temperature started rising from 38.05 ºC and took 70 mins to reach the first 60.17 ºC, and then fluctuated between 50 ºC and 60 ºC every 32 to 40 mins. The heating periods of LSMHS on 13th Feb were obviously shorter than those on 5th Jan because of the warmer outdoor temperature. Eventually, the average HP outlet temperature was 56.5 ºC, and the average FC inlet temperature was 55.32 ºC on 13th Feb. The operation mode of LSMHS in Feb is identical to that of Jan due to the low solar radiation, but it had shorter operation times in the warmer weather of Feb.

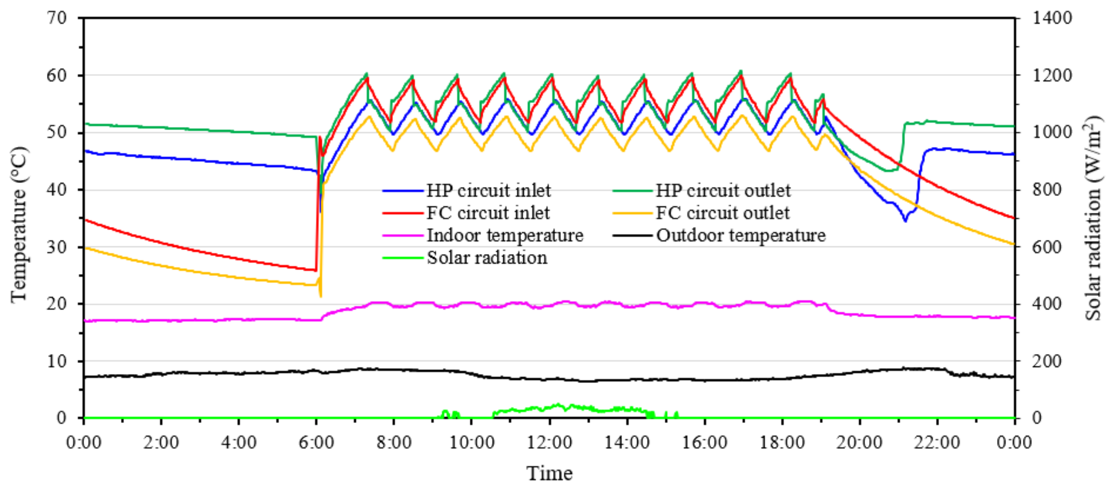

Figure 16. Operation conditions of the LSMHS on 13th Feb 2022

Figure 17 illustrates the practical system performance on 13th Feb. The heating capacity of LSMHS was still totally dependent on the THRHP because of insufficient solar radiation. Compared to the system performance on 5th Jan, the system heating capacity rose on 13th Feb, ranging from 27000 W to 34300 W because of warmer ambient, while the system heat supply was similar owing to the same water temperature and indoor temperature. Eventually, the total HD of the LSMHS achieved 223.98 kWh on 13th Feb, which was reduced by 30.20% compared to that of 5th Jan.

Regarding the system power consumption, it had the same characteristics found on 5th Jan because the power consumption of THRHP was mainly affected by water temperature but not outdoor temperature [15], and thus still fluctuated between 11779 W and 14830 W. However, with the warmer ambience and lower heat demand of the workshop, the operation time of LSMHS was reduced. Thus, although the power consumption of LSMHS was not decreased, the total energy consumption of LSMHS on 13th Feb diminished by 41.62% when compared to that of 5th Jan, only 99.62 kWh. Benefiting from the higher heating capacity on the warmer day, the COP_{sys} of LSMHS was promoted, ranging from 2.05 to 2.56 and averaging at 2.25 on 13th Feb.

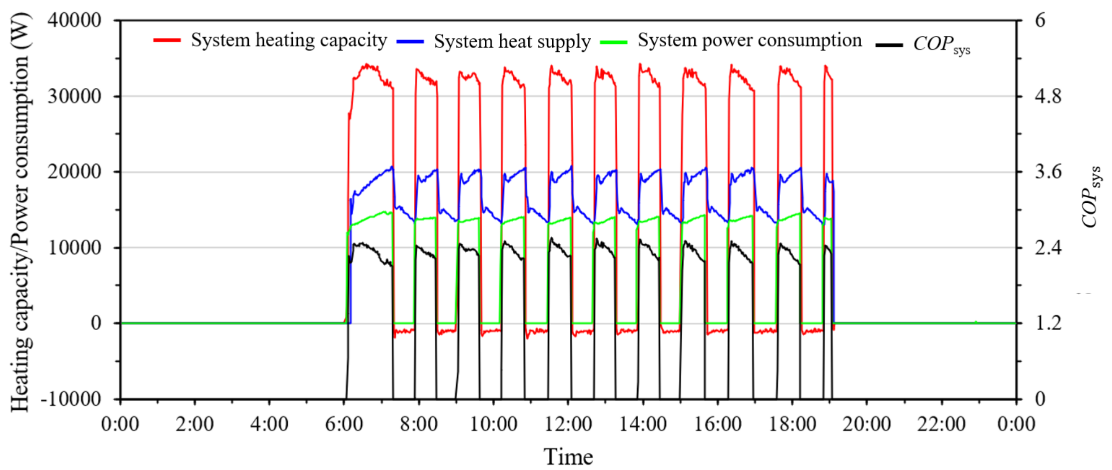

Figure 17. Practical performances of the LSMHS on 13th Feb 2022

4.2.3. Practical operation of the LSMHS in Mar

Figure 18 shows the practical operation performances of the LSMHS in Mar. The daily system heat production ranged from 66.34 kWh to 368.76 kWh as depicted in Figure 18 (a). As the weather got warmer and solar radiation grew stronger, the daily system energy consumption ranged from 25.45 kWh to 175.38 kWh in Mar, which was lower than those of Feb as shown in Figure 18 (b). To further analyze the practical operation characteristics and performances of the LSMHS in Mar, the most representative day of Mar is carefully discussed concerning system operation modes and heating performance changes. More insights into the system's operation and characteristics are disclosed in practical application as follows.

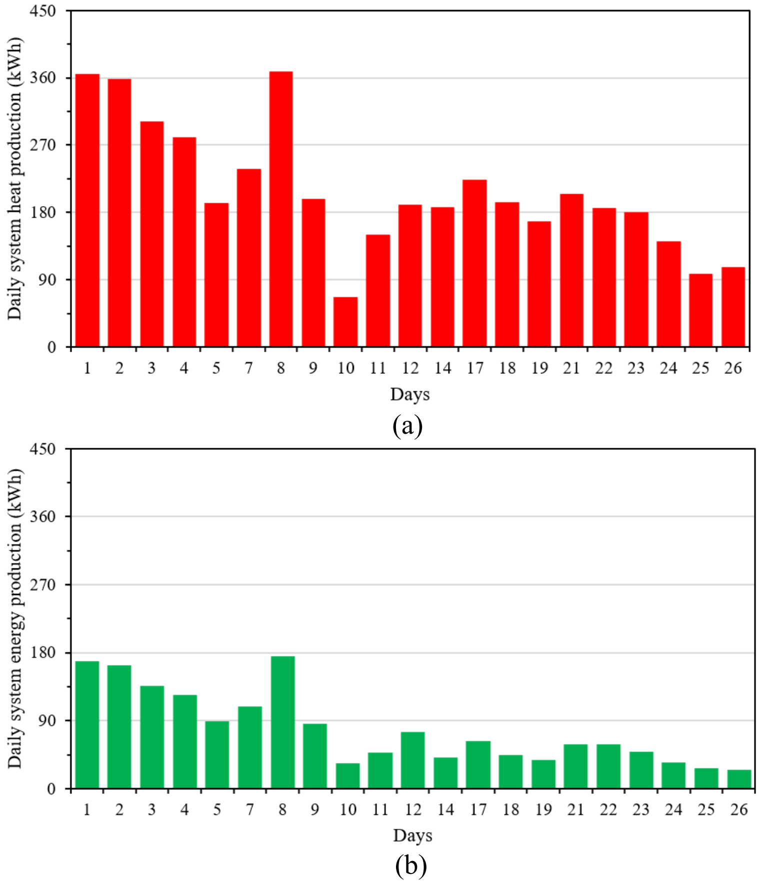

Figure 18. Practical operation results of the LSMHS in Mar (a) System heat production (b) System energy consumption

Figure 19 depicts the typical operation conditions of LSMHS on a day of Mar. The outdoor temperature of 17th Mar increased from 3.82 ºC and peaked at 19.81 ºC at 11:11. The average outdoor temperature of 17th Mar was up to 13.57 ºC, which was 9.61 ºC and 6.70 ºC higher than that of 5th Jan and 13th Feb, respectively. The solar radiation was strong and durable on 17th Mar, which was high up to 1042.00 W/m^2 in the midday and reached an average value of 447.05 W/m^2. The outdoor temperature and solar radiation on 17th March were good enough to support the SC circuit operation. Respecting the indoor temperature, it started increasing from 17 ºC when the THRHP operated and accelerated growth when the MFSC arrays kicked in. The indoor temperature kept rising and achieved its highest of 23.72 ºC with an average value of 21.42 ºC on 17th Mar.

From the water temperature results of 17th Mar, the operation characteristics of LSMHS were different from those of Jan and Feb. The LSMHS ran the THRHP only to heat water from 19.92 ºC at 7:00 when the solar radiation was 66.92 W/m^2. This is called THRHP mode. In the THRHP mode, the LSMHS absorbed heat from two sources, i.e., the outdoor air and indoor exhaust air to produce hot water for the FC circuit to warm the workshop.

When the solar radiation increased to 410.33 W/m^2 at 8:36, the LSMHS ran the MFSC arrays integrating with the THRHP and turned into its second mode, i.e., integration mode. During this period, the LSMHS had three heat sources, which were cold outdoor air, warm indoor exhaust air and strong solar radiation, and the water temperature increased the fastest in this mode.

Then, the LSMHS switched off the THRHP at 9:43 when the THRHP touched its upper water outlet temperature limit of 60 ºC. Afterwards, the MFSC arrays kept raising the SC circuit outlet temperature with solar radiation and achieved the highest temperature of 73.09 ºC at 12:38. The outdoor air temperature was 15.53 ºC at 12:38, and thus the MFSC arrays worked at conditions of high normalized temperature of 0.0593 K/(W/m^2). In this third mode, which was called MFSC mode, the LSMHS only had one heat source, i.e., strong solar radiation.

After that, the cloud shadowed the sun, so the SC circuit was switched off. The LSMHS turned back to the THRHP mode when the water temperature dropped to 50 ºC and then kept the HP circuit outlet temperature between 50 ºC and 60 ºC. As a result, the highest FC inlet temperature was 60.73 ºC on this typical sunny day, which was higher than that of Jan and Feb.

To sum up, the LSMHS operated in three modes throughout the day and changed the heat sources according to the weather conditions. The average HP circuit outlet temperature was 49.98 ºC, the average SC circuit outlet temperature was 64.98 ºC, and the average FC inlet temperature was 43.18 ºC on 17th Mar.

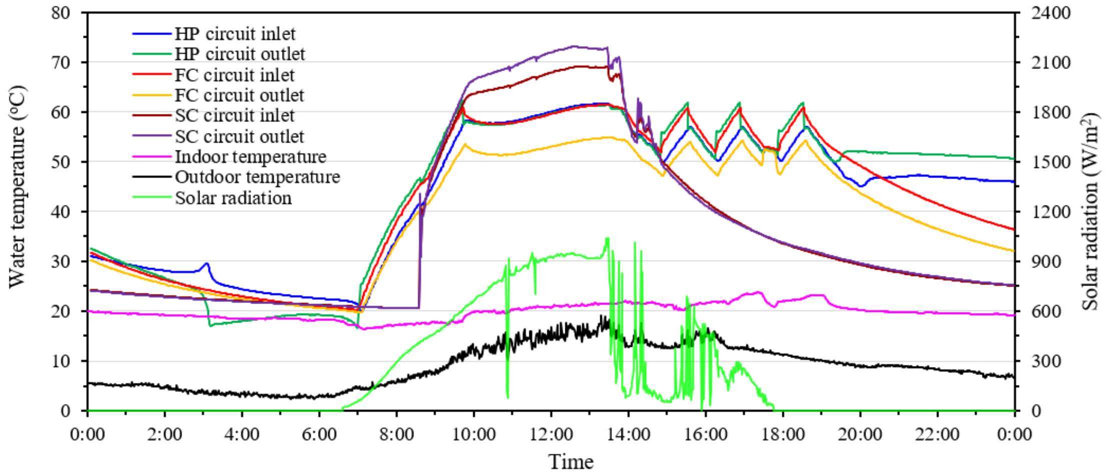

Figure 19. Operation conditions of the LSMHS on 17th Mar 2022

Figure 20 illustrates the system heating capacity of the LSMHS on 17th Mar. The system heating capacity had different compositions in different modes. In the TRHRP mode, the system heating capacity was equal to the HP heating capacity produced by the THRHP. Thus, the system heating capacity gradually decreased from 31600 W to 28300 W during this period as the water temperature rose and heat loss increased.

When the LSMHS turned into the integration mode as solar radiation grew, the MFSC arrays started collecting solar heat energy. The SC circuit was a closed circuit that needed to release solar heat energy to the water tanks by the immersion heat exchangers. At the beginning of this mode, the SC circuit outlet temperature was lower than the HP circuit inlet temperature. Therefore, the SC circuit could not release solar heat energy to the tanks but extracted heat from the tanks when it was collecting solar radiation. And thus, the SC heating capacity had a sharp increase from 0 to 13567 W at the beginning of the integration mode. As the SC circuit outlet temperature went up and surpassed the HP circuit inlet temperature, the MSFC arrays released solar heat energy to the water tanks, and the HP water temperature rose much more quickly. As a result, the system heating capacity climbed up as the solar radiation increased, which reached a maximum of 40300 W. At the same time, the solar thermal efficiency of the MFSC arrays reached 25.52% at the end of integration mode, when the normalized temperature of the MFSC was 0.085 $K/(W/m^2)$.

Then, the LSMHS switched to the MFSC mode when the HP outlet temperature reached 60 ºC and the THRHP stopped. However, the HP circuit water pump kept running because of the anti-frosting program, so the HP heating capacity was negative, which was around -1800 W during this period. As for the SC circuit, the SC heating capacity increased with solar radiation, ranging from 10000 W to 23000 W. The solar thermal efficiency of MFSC arrays peaked at 39.05% on 17th Mar when the normalized temperature was 0.064 $K/(W/m^2)$. Afterwards, the solar radiation dropped, and the LSMHS ran the THRHP mode again to maintain the HP water outlet temperature between 50 ºC and 60 ºC. The system heating capacity varied between 28300 W and 35100 W.

As for the system heat supply ability, it changed with the FC inlet temperature which grew quickly from 4000W to 21700W during the THRHP mode and integration mode, and then was stable around 16700 W to 18200 W during the MFSC mode. Thereafter, the system heat supply fluctuated between 12600 W and 20300 W during the last THRHP mode.

To sum up, the LSMHS operates the THRHP to heat water during periods of cloudy, and integrates the MFSC arrays with THRHP during periods of lower water temperature (< 60 ºC) and sunny. In conditions of high water temperature (> 60 ºC) and sunny, the LSMHS fully depends on the MFSC arrays to maintain the water temperature. The total heat production of the LSMHS achieved 224.08 kWh on 17th Mar, in which the MFSC arrays contributed to 39.38% (88.24 kWh), and the THRHP occupied 60.62% (135.84 kWh). The average solar thermal efficiency of the MFSC arrays achieved 26.62% at the practical conditions of a high average SC circuit outlet temperature of 64.98 ºC and a low average ambient temperature of 13.57 ºC.

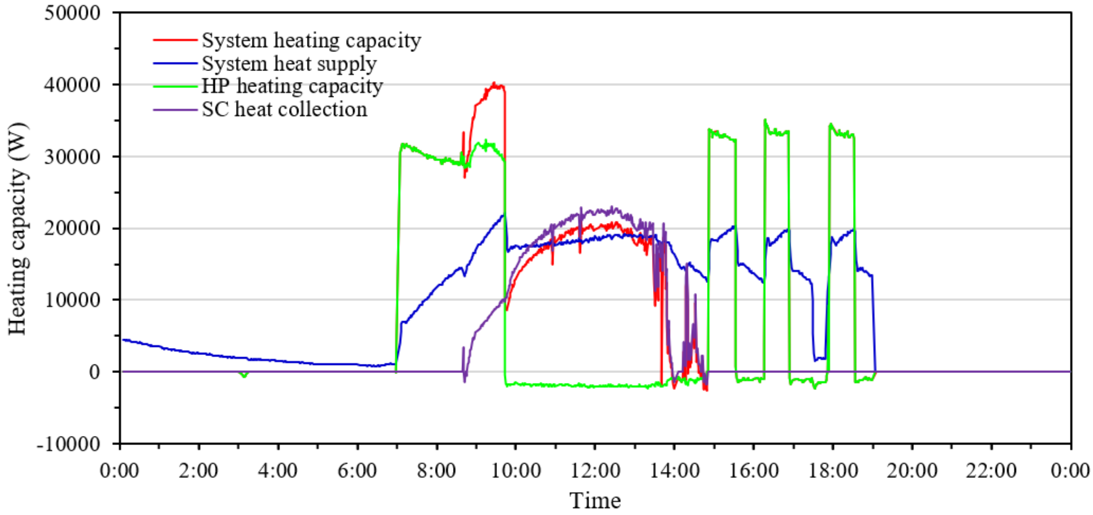

Figure 20. Heating capacity of the LSMHS on 17th Mar 2022

Figure 21 shows the power consumption of the LSMHS, in which the operation time of THRHP was significantly reduced, only allocating at the cloudy period of the beginning and end of the day. The system power consumption increased with the HP circuit water outlet temperature in these periods, ranging from 8919.944 W to 14733.17 W. In the MFSC mode, the power consumption dramatically diminished to around 814 W. The LSMHS automatically minimized the operation of THRHP and maximized the proportion of the MFSC arrays by switching operation modes according to weather. The total energy consumption of LSMHS eventually reached 63.19 kWh on 17th Mar, while the occupation of the THRHP was 91.19% (57.62 kWh). The daily energy consumption of LSMHS on 17th Mar was significantly reduced by 36.57% when compared to that of 13th Feb.

As a result, the COP_{sys} of LSMHS ranged between 2.21 to 3.54 in the THRHP mode, and stable around 2.44 to 2.91 during the integration mode. And afterwards, the COP_{sys} of LSMHS jumped to the most efficient range of 7.85 to 26.02 in the MFSC mode. Lastly, the $COP_{sys,ave}$ of LSMHS was average at 3.55 on 17th Mar, which was 57.73% higher than that of 13th Feb.

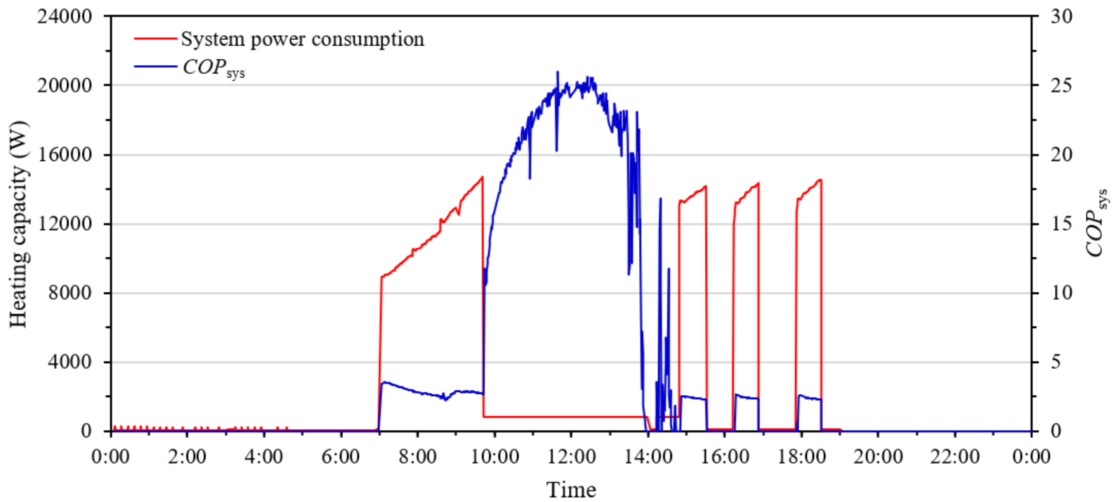

Figure 21. Heating performances of the LSMHS on 17th Mar 2022

4.3. Practical heating and eco-economic performances of the LSMHS

The practical heating performance and eco-economic performance of the LSMHS are analyzed at monthly level and compared to the library's original gas boiler heating system (GBHS).

4.3.1 Heating performances of the LSMHS

Figure 22 summarizes the practical conditions of the LSMHS in the three operation months, which were concluded from the data of 68 practical operation days. It clearly illustrates that the working conditions were changed in the three months. The monthly average outdoor temperature increased quickly from 3.41 ºC in Jan to 11.67 ºC in Mar, while the average indoor temperature rose steadily with outdoor temperature and stayed above 20 ºC in all months. The results of the monthly average indoor temperature fully proved the feasibility of the LSMHS when it directly replaced the library’s original gas boiler heating system without retrofitting the heating terminals.

As for the monthly average water temperature of the three circuits, the monthly average HP circuit outlet temperatures were close, which reached 56.99 ºC, 56.57 ºC and 55.63 ºC in Jan, Feb and Mar, respectively. Regarding the SC circuit, the MFSC arrays did not operate in cold and cloudy months, having no SC circuit water flowing out in Jan and Feb. Therefore, the SC circuit water outlet temperature was not available in Jan and Feb and was not shown in comparison. When the average solar radiation significantly jumped to 340.06 W/m^2 in Mar, the MFSC arrays collected abundant solar energy and achieved a monthly average SC circuit water outlet temperature of 67.72 ºC. As a result, the average water inlet temperatures of the FC circuit were respectively 54.27 ºC and 54.33 ºC in Jan and Feb, which were nearly identical. And then, it grew to 56.15 ºC in Mar because of the high water outlet temperature of the SC circuit.

In summary, the LSMHS extracted heat from cold outdoor air and warm exhaust air to produce high-temperature water for building heating. When the solar radiation was strong, the LSMHS gained more heat from three different sources, i.e., solar radiation, outdoor and exhaust air, which were switched and integrated according to the water temperatures.

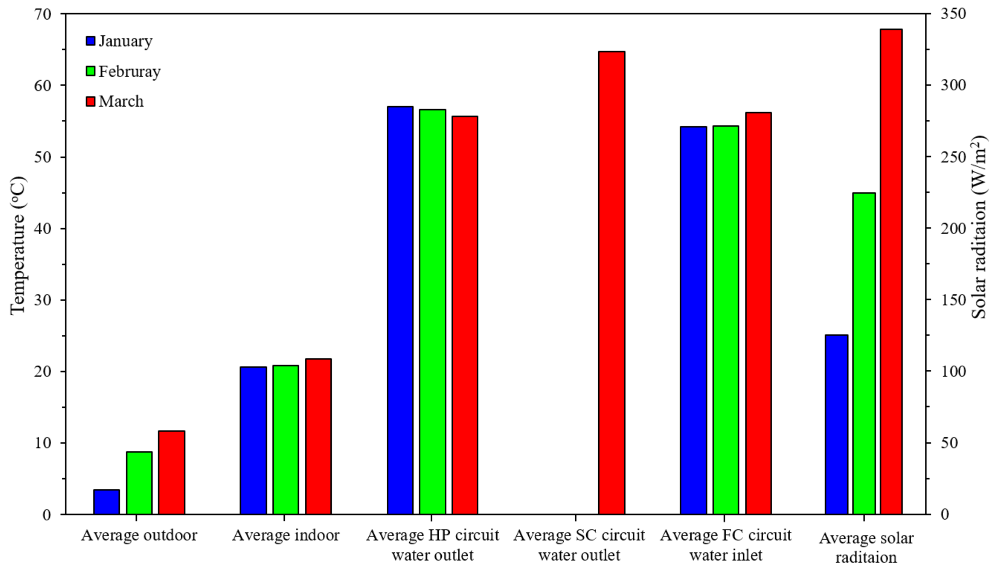

Figure 22. Practical operation conditions of the LSMHS in demonstration months

Figure 23 depicts the heating performance of the LSMHS. The heat production of the LSMHS came from the heat generation of the THRHP and the heat collection of the MFSC arrays. The heat productions of the LSMHS were 8533.55 kWh, 5739.01 kWh and 4454.44 kWh in Jan, Feb and Mar, respectively, which were reduced by 32.75% and 22.38% as the outdoor temperature gradually rose from Jan to Mar. The MFSC arrays achieved an average solar thermal efficiency of 21.63% and contributed 25.65% of the total system heat production in Mar. Thus the heat generation of THRHP was significantly reduced to 3311.68 kWh in Mar.

Different from heating production, The energy consumption of the LSMHS mainly came from the THRHP in all months. As shown in Figure 23, the heating energy consumptions of THRHP were 3959.94 kWh, 2588.80 kWh, and 1549.48 kWh in Jan, Feb and Mar, which were responsible for 98.33%, 98.34% and 93.20% of the system energy consumption respectively. Besides, the energy consumption of THRHP defrosting only had 0.74 kWh (0.02%), 1.81 kWh (0.07%) and 0.96 kWh (0.06%) in each month, fully proving that the novel defrosting method of THRHP had negligible defrosting consumption. Notably, the SC circuit only consumed 68.06 kWh of electricity but produced 1142.77 kWh of heat in Mar, which had a very high energy efficiency and was the key promotion to the system performance. Eventually, the system energy consumptions were 4027.38 kWh, 2632.53 kWh and 1662.54 kWh in Jan, Feb, and Mar, respectively, which decreased by 34.61% and 36.91% as the ambient went warmer and solar radiation grew stronger.

Eventually, the monthly average $COP_{sys,ave}$ of LSMHS also increased from Jan to Mar as the outdoor temperature and solar radiation grew, reaching 2.12, 2.18 and 2.68, respectively. It was worth noting that the LSMHS benefits more from the two-stage heat recovery structure in colder ambient. The $COP_{sys,ave}$ of LSMHS on Jan only 2.77% lower than that on Feb when the average outdoor temperature of Jan was 5.29 °C colder than that of Feb. This advantage further indicates that the LSMHS is suitable for low ambient temperature operation. Furthermore, when the MFSC arrays cooperated with the THRHP in Mar, the $COP_{sys,ave}$ significantly ascended by 23.04%.

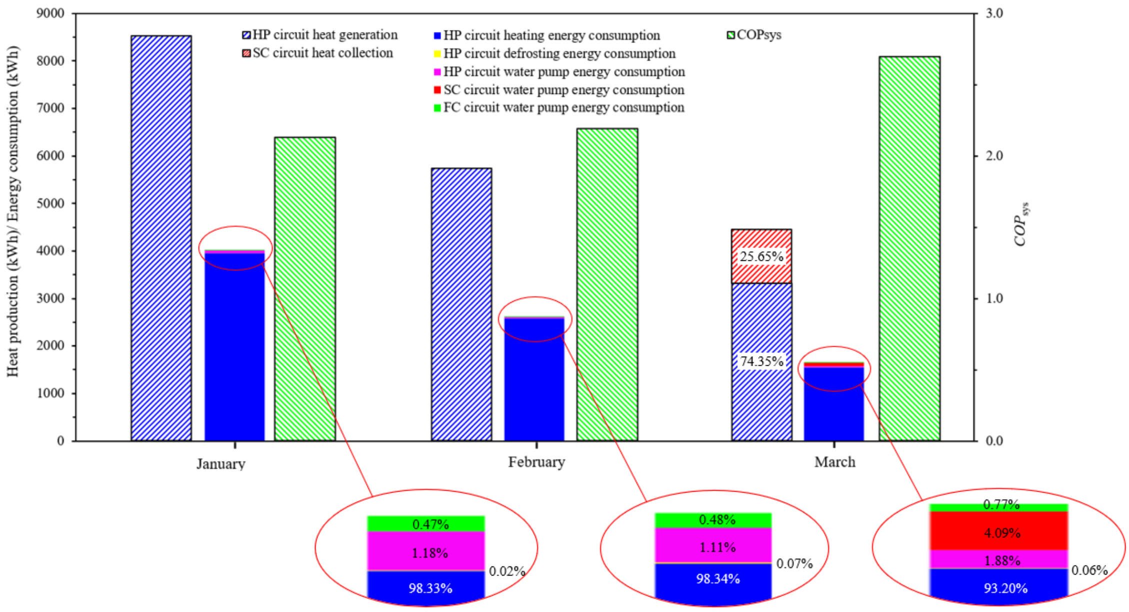

Figure 23. Practical heating performance of the LSMHS in demonstration months

4.3.2. Eco-economic performance of the LSMHS

According to the energetic performance results, the eco-economic performance of the system is further analyzed by comparing it to the library's original GBHS. The original GBHS system had no monitoring subsystem, and thus, the comparison assumed that the average efficiency of the original GBHS is 85% according to Ref [21]. Furthermore, considering the peak and off-peak times, the electricity price of the Hull Central Library was £0.22625/kWh during the off-peak period from 1:00 to 8:00 and rose to £0.30074/kWh during the peak period. The gas price was constant at £0.10774/kWh all the time. The carbon emissions factor of the UK electricity and natural gas are derived from the climate transparency report of G20 countries [22] and the greenhouse gas reporting [23], which are 0.176 kg/kWh and 0.183 kg/kWh, respectively. To meet the heating requirement of the workshop under the same environmental conditions, the heat production of GBHS is assumed to be equal to that of the LSMHS.

Figure 24 shows the eco-economic performance of the practical demonstration of the LSMHS. The heating bill of the LSMHS was £1135.23 in Jan. This was 4.95% higher than using GBHS, of which the heating bill was £1081.68. However, benefiting from the high COP_{sys} of LSMHS and low carbon emission factor of electricity energy, the LSMHS produced very low carbon dioxide of 708.49 kg, while the GBHS would emit 1837.22kg, significantly declining the carbon emission by 61.44%.

As the weather got warmer in Feb, due to the increased monthly average $COP_{sys,ave}$ of LSMHS and obvious reduction of operation time, the LSMHS reduced the heating bill to £746.49, which was 34.24% lower than that of Jan. As a result, although the Feb heating bill of the LSMHS was still 2.62% higher than using GBHS, the LSMHS further reduced its carbon emission by 34.61% compared to that of Jan. Eventually, the LSMHS emitted 62.50% lower carbon dioxide than the GBHS in Feb.

When the weather became sunny in Mar, the cooperation of the MFSC arrays and THRHP improved the monthly average COP_{sys} by 23.04%, and thus the heating bill of the LSMHS significantly declined by 36.40% compared to that of Feb, costing only £474.76 in Mar and achieving a 15.92% bill saving when compared to the GBHS. Furthermore, the carbon emission of LSMHS further declined by 36.92% from Feb, and achieved the maximum carbon reduction of 69.52% compared to the GBHS in Mar.

Eventually, as shown in Table 3, the three-month demonstration of the novel LSMHS generated 18727.00 kWh of heat and consumed 8318.52 kWh of electricity, achieving the average $COP_{sys,ave}$ of 2.25 in practical application, which was more energy-efficient than the GBHS by improving the system efficiency by 164.71%. More importantly, the three-month demonstration of the LSMHS reached a bill saving of 0.73% with a significant carbon reduction of 63.69% when compared to the GBHS, meaning that the LSMHS can achieve an equivalent bill saving of £6.7 when it reduces every tone of carbon emission. These advantaged eco-economic performances of the LSMHS were essential to accelerate the wide application of low-carbon heating systems and helped the government deliver the carbon-neutral targets.

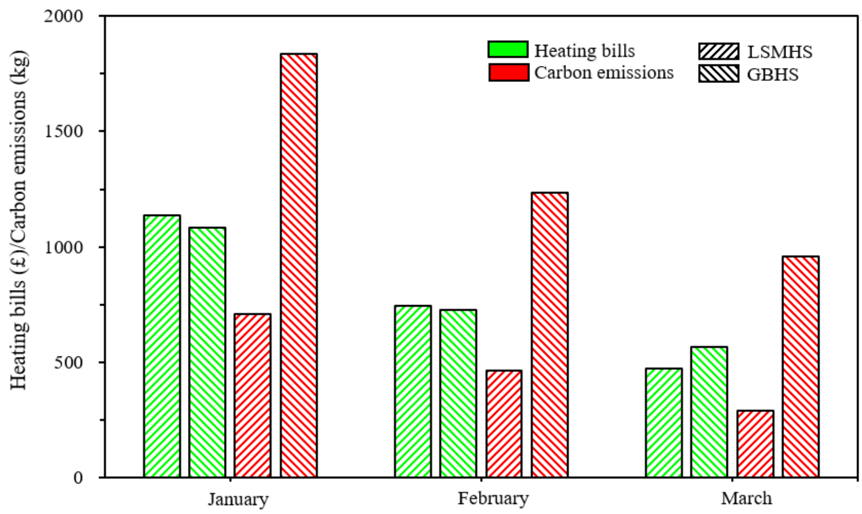

Figure 24. Practical eco-economic performances of the LSMHS in demonstration months

Table 3. Comparison of system performances in the three-month demonstration

	LSMHS	GBHS
Total heat production (kWh)	18727.00	18727.00
Total energy consumption (kWh)	8318.52 (electricity)	22031.76 (gas)
Average COP_{sys}	2.25	0.85
Total heating bill (£)	2356.48	2373.77
Total carbon emission (kg)	1464.06	4031.81

4.4 Further remarks

From the practical demonstration of LSMHS in the Hull Central Library, it is proved that the LSMHS has good heating performances to achieve heating bill savings and provide great carbon reductions when compared to GBHS. With the introduction of the carbon tax policy [24], the LSMHS can attract more attention from the market through carbon reduction grants. In addition, the photovoltaic panel is another option for the low-carbon heating system compared to the MFSC, which can directly convert solar radiation into electricity but at a lower conversion efficiency. To fully explore the application potential of the LSMHS, it needs to develop detailed model validation, simulation, and comparison in future research.

5. Conclusions

The MFSC array and LSMHS are first proposed and applied to the Hull Central Library in practical demonstration. The operating performance of the MFSC array and LSMHS are disclosed in the real-life application, and the eco-economic performance of the LSMHS is analyzed and further compared to the traditional gas boiler heating system, revealing the advantages and application potential of the low-carbon heating technologies, which are concluded as follows:

1. The MFSC arrays had a good heat performance in conditions of high normalized temperature, which ranged from 0.0479 to 0.1382 $W/m^2/K$ in the practical application. The highest solar thermal efficiency of the MFSC arrays peaked at 48.97% when the water outlet temperature was 69.14 ºC and the normalized temperature was 0.0589 $W/m^2/K$.

2. The novel LSMHS integrated the MFSC arrays with THRHP, successfully maximizing the advantages of each component. When the solar radiation was high, the LSMHS ran integration mode, which integrated the MFSC with THRHP to quickly increase water temperature until 60 ºC, fast responding to building heat load. In this mode, the MFSC arrays performed good solar thermal efficiency at the conditions of high water temperatures and cold ambient temperatures, effectively reducing the operation time of THRHP. When the water temperature surpassed 60 ºC, the LSMHS turned into MFSC mode, which operated the MFSC arrays alone to save energy and maximize the efficiency advantages of MFSC arrays. When solar radiation was low, the LSMHS ran THRHP mode. The THRHP worked alone to maintain the water temperature between 50 ºC and 60 ºC, which had performance advantages of high heating capacity and COP at cold ambient conditions.

3. The LSMHS had significant declines in heating production and energy consumption when the monthly average outdoor temperature increased from 3.41 ºC of Jan to 8.70 ºC of Feb, and its monthly average $COP_{sys,ave}$ achieved 2.12 and 2.18 in Jan and Feb, respectively. Benefiting from the two-stage heat recovery structure of THRHP, the COP_{sys} of LSMHS maintained stability as ambient temperature obviously decreased. When the monthly average solar radiation rose to 340.06 W/m^2, the MFSC arrays contributed 25.65% of total system heat production, and thus, the monthly average COP_{sys} of LSMHS ascended to 2.68 in Mar.

4. The LSMHS had 4.95% and 2.62% higher heating bills than GBHS in Jan and Feb owing to the obvious lower gas price in the UK. With the utilization of solar energy and high COP_{sys}, the LSMHS achieved 15.92% bill saving in Mar when compared to the GBHS, and thus eventually obtained a 0.73% bill saving in the three-month demonstration. Most importantly, the LSMHS provided 61.44% to 69.52% carbon reductions in different weather conditions, eventually achieving £6.7 bill saving when it reduced every tone of carbon emission.

Acknowledge

This work is funded by the UK BEIS project ‘A low carbon heating system for existing public buildings employing a highly innovative multiple-throughout-flowing micro-channel solar-panel-array and a novel mixed indoor/outdoor air source heat pump’ (LCHTIF1010). This work is also sponsored by the Chinese Scholarship Council.

Reference

[1] Renewables 2019 - Analysis and forecast to 2024. International Energy Agency, https://www.iea.org/reports/renewables-2019, 2019.

[2] Carbon Reduction Policy. Crown Commercial Service, https://www.gov.uk/government/publications/carbon-reduction-policy/carbon-reduction-policy, 2023.

[3] UK becomes first major economy to pass net zero emissions law. Department for Business, Energy & Industrial Strategy, https://www.gov.uk/government/news/uk-becomes-first-major-economy-to-pass-net-zero-emissions-law, 2019.

[4] Hull 2030 Carbon Neutral Strategy. Hull City Council, https://www.hull.gov.uk/environment/pollution/hull-2030-carbon-neutral-strategy, 2019.

[5] S. Sadhishkumar, T. Balusamy. Performance improvement in solar water heating systems—A review. Renewable and Sustainable Energy Reviews. 37 (2014) 191-8.

[6] D.L. Loveday, C. Craggs. STOCHASTIC MODELING OF TEMPERATURES AFFECTING

THE INSITU PERFORMANCE OF A SOLAR-ASSISTED HEAT-PUMP - THE UNIVARIATE APPROACH. Sol Energy. 49 (1992) 279-87.

[7] S.K. Chaturvedi, T.O. Mohieldin, D.T. Chen. 2ND-LAW ANALYSIS OF SOLAR-ASSISTED HEAT-PUMPS. Energy. 16 (1991) 941-9.

[8] L.W. Yang, R.J. Xu, N. Hua, Y. Xia, W.B. Zhou, T. Yang, et al. Review of the advances in solar-assisted air source heat pumps for the domestic sector. Energy Conv Manag. 247 (2021).

[9] J. Cai, Z. Li, J. Ji, F. Zhou. Performance analysis of a novel air source hybrid solar assisted heat pump. Renew Energy. 139 (2019) 1133-45.

[10] C. Tzivanidis, E. Bellos, G. Mitsopoulos, K.A. Antonopoulos, A. Delis. Energetic and financial evaluation of a solar assisted heat pump heating system with other usual heating systems in Athens. Appl Therm Eng. 106 (2016) 87-97.

[11] Y. Jiang, H. Zhang, Y. Wang, Y. Wang, M. Liu, S. You, et al. Research on the operation strategies of the solar assisted heat pump with triangular solar air collector. Energy. 246 (2022).

[12] C. Huan, S. Li, F. Wang, L. Liu, Y. Zhao, Z. Wang, et al. Performance Analysis of a Combined Solar-Assisted Heat Pump Heating System in Xi'an, China. Energies. 12 (2019).

[13] L.W. Yang, N. Hua, J.H. Pu, Y. Xia, W.B. Zhou, R.J. Xu, et al. Analysis of operation performance of three indirect expansion solar assisted air source heat pumps for domestic heating. Energy Conv Manag. 252 (2022) 115061.

[14] M. Song, S. Deng, C. Dang, N. Mao, Z. Wang. Review on improvement for air source heat pump units during frosting and defrosting. Appl Energy. 211 (2018) 1150-70.

[15] Y. Li, Z. Li, Y. Fan, C. Zeng, Y. Cui, X. Zhao, et al. Experimental investigation of a novel two-stage heat recovery heat pump system employing the vapor injection compressor at cold ambience and high water temperature conditions. Renew Energy. 205 (2023) 678-94.

[16] ASHRAE. Ventilation for Acceptable Indoor Air Quality. 2019.

[17] G. Faure, M. Vallée, C. Paulus, T.Q. Tran. Impact of faults on the efficiency curve of flat plate solar collectors: a numerical analysis. J Clean Prod. 231 (2019) 794-804.

[18] M.C. Rodríguez-Hidalgo, P.A. Rodríguez-Aumente, A. Lecuona, G.L. Gutiérrez-Urueta, R. Ventas. Flat plate thermal solar collector efficiency: Transient behavior under working conditions. Part I: Model description and experimental validation. Appl Therm Eng. 31 (2011) 2394-404.

[19] A. Ege, H.M. Şahin. Uncertainties in energy and exergy efficiency of a High Pressure Turbine in a thermal power plant. International Journal of Hydrogen Energy. 41 (2016) 7197-205.

[20] A. Shirazi, S. Pintaldi, S.D. White, G.L. Morrison, G. Rosengarten, R.A. Taylor. Solar-assisted absorption air-conditioning systems in buildings: Control strategies and operational modes. Appl Therm Eng. 92 (2016) 246-60.

[21] C. Mahon, M.K. Mediboyina, D. Gartland, F. Murphy. Life cycle assessment of Irish district heating systems: a comparison of waste heat pump, biomass-based and conventional gas boiler. Clean Technologies and Environmental Policy. 24 (2022) 1437-51.

[22] The Climate Transparency Report 2021. Climate Transparency, https://www.climate-transparency.org/g20-climate-performance/g20report2021#1531904804037-423d5c88-a7a7, 2021.

[23] Greenhouse gas emission intensity of electricity generation in Europe. European Environment Agency, https://www.eea.europa.eu/ims/greenhouse-gas-emission-intensity-of-1, 2021.

[24] Carbon Emissions Tax. HM Revenue & Customs and HM Treasury, https://www.gov.uk/government/consultations/carbon-emissions-tax, 2021.